

Article

Discovery of Novel Small-molecule Inhibitors of Nuclear Factor- κ B Signaling with Anti-inflammatory and Anti-cancer Properties

Lei Zhang, Lei Shi, Shafer Soars, Joshua Kamps, and Hang Hubert Yin

J. Med. Chem., **Just Accepted Manuscript** • DOI: 10.1021/acs.jmedchem.7b01557 • Publication Date (Web): 05 Jun 2018

Downloaded from <http://pubs.acs.org> on June 5, 2018

Just Accepted

"Just Accepted" manuscripts have been peer-reviewed and accepted for publication. They are posted online prior to technical editing, formatting for publication and author proofing. The American Chemical Society provides "Just Accepted" as a service to the research community to expedite the dissemination of scientific material as soon as possible after acceptance. "Just Accepted" manuscripts appear in full in PDF format accompanied by an HTML abstract. "Just Accepted" manuscripts have been fully peer reviewed, but should not be considered the official version of record. They are citable by the Digital Object Identifier (DOI®). "Just Accepted" is an optional service offered to authors. Therefore, the "Just Accepted" Web site may not include all articles that will be published in the journal. After a manuscript is technically edited and formatted, it will be removed from the "Just Accepted" Web site and published as an ASAP article. Note that technical editing may introduce minor changes to the manuscript text and/or graphics which could affect content, and all legal disclaimers and ethical guidelines that apply to the journal pertain. ACS cannot be held responsible for errors or consequences arising from the use of information contained in these "Just Accepted" manuscripts.



ACS Publications

is published by the American Chemical Society, 1155 Sixteenth Street N.W., Washington, DC 20036

Published by American Chemical Society. Copyright © American Chemical Society. However, no copyright claim is made to original U.S. Government works, or works produced by employees of any Commonwealth realm Crown government in the course of their duties.

Discovery of Novel Small-molecule Inhibitors of Nuclear Factor- κ B Signaling with Anti- inflammatory and Anti-cancer Properties

Lei Zhang,^{1,‡} Lei Shi,^{1,2,‡} Shafer Myers Soars,¹ Joshua Kamps,¹ and Hang Yin^{1,}*

¹Department of Chemistry and Biochemistry and the BioFrontiers Institute, University of Colorado, Boulder, CO 80309, USA

²Jiangsu Key Laboratory of Drug Design and Optimization, Department of Medicinal Chemistry, China Pharmaceutical University, Nanjing 210009, PR China

[‡]Co-first author

*Correspondence: hubert.yin@colorado.edu

KEYWORDS. NF- κ B, high-throughput screening (HTS), drug discovery, anti-inflammatory, anti-cancer

ABSTRACT. Excessive NF- κ B activation contributes to the pathogenesis of numerous diseases. Small-molecule inhibitors of NF- κ B signaling have significant therapeutic potential especially in treating inflammatory diseases and cancers. In this study, we performed a cell-based high-throughput screening to discover novel agents capable of inhibiting NF- κ B signaling. Based on two hit scaffolds from the screening, we synthesized 69 derivatives to optimize the potency for inhibition of NF- κ B activation, leading to successful discovery of the most potent compound **Z9j** with over 170-fold enhancement of inhibitory activity. Preliminary mechanistic studies revealed that **Z9j** inhibited NF- κ B signaling via suppression of Src/Syk, PI3K/Akt and IKK/I κ B pathways. This novel compound also demonstrated anti-inflammatory and anti-cancer activities, warranting its further development as a potential multifunctional agent to treat inflammatory diseases and cancers.

INTRODUCTION

Nuclear factor- κ B (NF- κ B) is a master transcription factor that regulates a number of cellular activities such as immune responses, inflammation, and cell survival.¹ The mammalian NF- κ B family encompasses five members, including p50, p52, p65 (RelA), RelB, and c-Rel, which form various homo- or heterodimeric complexes. In unstimulated cells, NF- κ B dimer is sequestered in the cytoplasm by the inhibitory family protein I κ B in a latent form. Upon activation, different upstream pathways converge on the IKK complex which consists of two catalytic components, IKK α and IKK β , and a regulatory component named NF- κ B essential modulator (NEMO) or IKK γ .² IKK complex phosphorylates I κ B, leading to its subsequent ubiquitination and degradation by the proteasome (**Figure 1A**). This releases NF- κ B dimer and allows it to translocate into the nucleus to activate specific target genes.^{3, 4}

A broad range of stimuli can activate NF- κ B signaling including pathogens, inflammatory cytokines, growth factors, ultraviolet, and oxidative stress.⁵ Upon activation of distinct stimuli, many membrane receptors can initiate various signaling pathways that culminate in the activation of NF- κ B, for example Toll-like receptors (TLRs), tumor necrosis factor receptor (TNFR), interleukin-1 receptor (IL-1R), T cell receptor (TCR), and B cell receptor (BCR) (**Figure 1A**).⁶⁻⁸ Among these, TLRs are the best studied receptors.^{9, 10} The human TLR family to date consists of ten members which recognize a wide range of pathogen-associated molecular patterns (PAMPs) or danger-associated molecular patterns (DAMPs), such as bacterial lipoproteins (TLR2 ligand), viral double-stranded RNA (TLR3 ligand), lipopolysaccharide (LPS; TLR4 ligand), flagellin (TLR5 ligand), viral single-stranded RNA (TLR7 and 8 ligand), and bacterial CpG DNA (TLR9 ligand). In response to PAMPs or DAMPs, all TLR signaling pathways initiate inflammatory cascades, resulting in NF- κ B activation. The activation of NF- κ B

in turn controls the expression of hundreds of genes involved in immune responses, cell cycle, apoptosis, cell adhesion, tissue differentiation, and DNA repair.¹

Due to its key role as a master switch for many genes, it is not surprising that aberrant activation NF- κ B is associated with a plethora of disorders, especially inflammatory diseases and cancers.¹¹⁻¹⁴ Inflammation is an important defense system by which the body protects us from exogenous infections and endogenous damage. NF- κ B has been recognized as a pivotal regulator of inflammation.¹⁵ Upon activation of NF- κ B signaling, various pro-inflammatory cytokines, chemokines, and other mediators such as TNF- α and nitric oxide (NO) are expressed to remove pathogens or damage. However, excessive or chronic activation of NF- κ B causes detrimental inflammation and results in high levels of inflammatory mediators, contributing to pathogenesis of many inflammatory diseases, such as systemic lupus erythematosus, sepsis, atherosclerosis, rheumatoid arthritis, asthma, diabetes, and Alzheimer's disease.¹¹⁻¹⁴ Importantly, inhibition of NF- κ B signaling by pharmacological interventions can potentially prevent or alleviate all these chronic disorders.^{16, 17} Constitutive activation of NF- κ B has also been found in many cancer cells and causes drug resistance by increasing cell proliferation and inhibiting apoptosis.¹⁸⁻²⁰ Therefore, inhibition of NF- κ B overactivation by small-molecule inhibitors has been recognized as an advantageous strategy for cancer therapy.^{21, 22} In this regard, NF- κ B is an exciting therapeutic target for drug discovery and development.¹⁴

The dynamic NF- κ B regulatory network offers a multitude of promising options for developing therapeutic interventions.²³ Generally, NF- κ B inhibition can be achieved by targeting any step of the signaling cascades, such as blocking the binding of stimuli to membrane receptors at an early stage, interfering with an intracellular component of the cascade to stop the signal transduction (e.g. kinases, phosphatases, ubiquitination, IKK complex, nuclear translocation), or

1
2
3 suppressing the NF- κ B nuclear activity (e.g. DNA binding, acetylation or methylation of NF-
4 κ B).^{24, 25} However, currently there are few NF- κ B signaling inhibitors that are entering clinical
5
6 trials, suggesting an urgent need to develop novel agents to modulate NF- κ B signaling.^{26, 27}
7
8

9
10 To discover novel agents that could inhibit NF- κ B signaling, we herein conducted a cell-
11 based high-throughput screening (HTS) using TLR-mediated NF- κ B activation as a phenotypic
12 platform. Our efforts led to the discovery of twelve hits, two of which were selected in this study
13
14 for extensive structure-activity relationship (SAR) studies, affording the most potent compound
15
16 **Z9j** with over 170-fold enhancement of inhibitory activity. Furthermore, we carried out
17 preliminary studies to understand possible inhibitory mechanism of **Z9j** by both cellular and
18
19 molecular approaches. Meanwhile, to investigate whether the newly discovered modulator has
20
21 therapeutic potential, we explored its anti-inflammatory and anti-cancer activities.
22
23
24
25
26
27
28

29 RESULTS AND DISCUSSION

30

31
32 **Cell-based high-throughput screening.** HTS has been proven to be highly efficient in
33 identifying biologically active small molecules as candidates for further drug discovery and
34 development.²⁸ HTS assays typically can be divided into two categories: biochemical and cell-
35 based assays.²⁹ Hits discovered in a biochemical HTS cannot always translate into the same
36
37 response in a cellular context due to several limitations such as lack of cellular cofactors and
38
39 issues of membrane permeability. In contrast, a cell-based HTS can reveal multiple targets in cell
40
41 signaling, some of which cannot be captured in biochemical screening.²⁹ Given the multiple
42
43 pathways that can activate NF- κ B signaling, a cell-based HTS is particularly advantageous for
44
45 the discovery of novel NF- κ B inhibitors. Therefore, we conducted a cell-based HTS using TLR-
46
47 mediated NF- κ B activation as a phenotypic platform to discover small-molecule modulators that
48
49 can inhibit any step of NF- κ B signaling.
50
51
52
53
54
55
56
57
58
59
60

Our group has successfully established a robust HTS platform based on a TLR-overexpression system.³⁰ We modified the protocol in this study to accommodate for screening inhibitors of TLR-mediated NF- κ B activation. Because of their low cost, ease of culture, and good reliability, human embryonic kidney 293 (HEK293) cells have been extensively used as a bench-mark expression system for TLR signaling studies.³¹ The chemical library utilized in this study was the Maybridge HitFinder v11 library which encompasses 14,400 diverse small molecules. Since there is still a lack of small-molecule TLR7 inhibitors, the HEK293 cell line was co-transfected with the human TLR7 gene and a secreted embryonic alkaline phosphatase (SEAP) reporter gene placed under the control of an NF- κ B-inducible promoter. Therefore, through the HTS, we could expect either inhibitors of TLR7 itself or inhibitors of TLR7-mediated NF- κ B activation, both of which are of interest to drug discovery.

The screening was conducted in 384-well plates in duplicate with a Z' value of 0.74, an indicator of robustness of the screening procedure.³² Transfected HEK293 cells were stimulated with TLR7 agonist R848 before treating with library compounds at 30 μ M. Triptolide, a known NF- κ B inhibitor,^{33, 34} and blank (w/ 4% DMSO) were used as positive and negative controls, respectively (**Figure S1**). SEAP secretion in the cell supernatant was measured to indicate levels of TLR7-mediated NF- κ B activation by colorimetric QUANTI-Blue detection. After the screening, the data obtained were statistically distributed based on the root mean square (RMS) values as depicted in **Figure 1B**. From the HTS, twelve hits were identified, among which hit compounds **S3a** and **Z3a** were selected in this study for structural optimization and SAR studies. The two hits were selected based on two criteria. First, they are among the top list of the twelve identified hits based on potency. Second, both of these compounds are structurally similar with two aromatic rings attached to a hydrazide linker (**Figure 1C**).

SAR Studies. To explore SAR and identify more potent inhibitors of the TLR7-mediated NF- κ B activation, we designed and synthesized 31 derivatives of **S3a** and 38 derivatives of **Z3a**. All the compounds were synthesized in a straightforward fashion following the routes outlined in **Schemes 1-7**. The SAR studies were mainly focused on the bilateral aromatic rings of hit compounds **S3a** and **Z3a** while maintaining the central hydrazide scaffold. The NF- κ B inhibitory activity of all the compounds were examined in HEK hTLR7 cells by the SEAP assay. The inhibition percentages of all the compounds were initially tested at 40 μ M and those with more than 50% inhibition were further tested for half-maximal inhibitory concentration (IC₅₀) values.

For derivatives of hit **S3a**, we first examined the position effect of the trifluoromethyl groups on the phenyl ring (**Table 1**). It turned out that the para- substitution (**S3c**) was more favorable than meta- substitution (**S3a**), whereas ortho- substitution (**S3b**) led to diminished activity. We also investigated the role of the heteroaromatic ring, particularly the necessity of the two sp²-hybridized nitrogen atoms and the amino group of **S3a**. The results showed that the N1 of the pyrazine system of **S3a** is indispensable, as indicated by the loss of activity of **S3f** (**Table 1**). The other two nitrogen atoms are inessential as compound **S3i** lacking both still showed strong NF- κ B inhibitory activity. Absence of the amino group on the pyrazine ring abolished the activity (**Table 1**, **S3a** and **S3e**) whereas attaching an amino or hydroxyl group (**Table 1**, **S3d** and **S3h**) to the aromatic system recovered the activity, suggesting that a hydrogen-bond donor or electron-donating group could offset the electron deficiency caused by two sp²-hybridized nitrogen atoms compared to those with only one. Halogen substituents (**Table 1**, **S3j** and **S3k**) resulted in significant decrease of NF- κ B inhibitory activity, indicating intolerance of substituents on the pyrazine ring. The importance of the flexible hydrazide linker was evidenced by compounds **S4**

which displayed no inhibition possibly due to their more rigid structures (**Table 1**). Therefore, the following SAR studies were dedicated to the bilateral aromatic rings only.

Maintaining the aminopyrazine ring, we studied various substituted phenyl rings with a preference to para- substitution (**Table 2**). There appeared no obvious electronic effect of substituents on the phenyl ring, since either electron-withdrawing (e.g. **S10f**) or electron-donating (e.g. **S10g** and **S10h**) groups did not result in any significant difference in the activity. Replacing the phenyl ring with pyridine proved to be unfavorable (**S10k**). In addition, long-chained substitution was not tolerated exemplified by compound **S10l**.

Based on the two best heteroaromatic rings and four best substituted phenyl rings from above SAR studies, we explored their different combinations. As expected, the best heteroaromatic ring and the best substituted phenyl ring produced the most potent compound **S11e** among the derivatives of hit **S3a**, with an IC_{50} value of $7.9 \pm 0.5 \mu M$ (**Table 3**).

The structural optimization of hit **Z3a** was also focused on the bilateral aromatic rings (**Table 4**). Investigation of different heteroaromatic rings found that an sp^2 -hybridized nitrogen atom adjacent to the hydrazide linker is vital to maintain the NF- κ B inhibitory activity (**Table 4**, **Z3a** vs **Z3b** and **Z3d-Z3f**). Appropriate substituents on the thiazole ring improved the activity (**Table 4**, **Z3a** vs **Z3c**).

Investigation of different substituted phenyl rings revealed a position effect of substituents with a preference for the para- position (**Table 5**, **Z3a** vs **Z5a** and **Z5b**). No obvious electronic or hydrogen-bonding effects were observed based on compounds **Z5c-Z5k**. However, replacing the phenyl ring with 2-pyridyl ring yielded a more potent compound **Z5l** compared with hit compound **Z3a**.

Maintaining the 2-pyridyl ring on the right side of the molecule, we then examined the aliphatic 2-isopropyl (**Z7a**), phenyl (**Z7b**), and heteroaromatic (**Z7c** and **Z7d**) substituents on the thiazole (**Table 6**). It turned out that the phenyl substituted compound **Z7b** resulted in significant improvement of TLR7-mediated NF- κ B inhibitory activity.

From **Z7b**, we further explored whether installing appropriate substituents on its phenyl ring would improve the inhibitory activity (**Table 7**). A trend for electronic effect of substituents on the phenyl ring was not identified, both electron-withdrawing (**Z9c**) and electron-donating (**Z9d-Z9h**) groups gave comparable activities. However, di-chloro substituted derivatives **Z9i-Z9k** displayed significant increase of inhibitory activities. Among them, compound **Z9j** (**CU-CPT-Z9j**) was the most potent compound with an IC_{50} value of $0.26 \pm 0.05 \mu\text{M}$. In this structure, the thiazole nitrogen is essential to maintain the activity, hydrophobic 2,4-dichlorophenyl substitution on the thiazole ring significantly improved the potency, and pyridine-2-carbohydrazide structure of **Z9j** is beneficial to the NF- κ B inhibitory activity. In comparison to its original hit **Z3a** ($44.8 \pm 0.9 \mu\text{M}$), compound **Z9j** showed over 170-fold enhancement of inhibitory activity to TLR7-mediated NF- κ B activation. Therefore, compound **Z9j** was selected for further biological studies.

Mechanism of Action Studies. We began the biological investigations of **Z9j** by examining its NF- κ B signaling inhibitory mechanism using cellular approaches. To determine whether **Z9j** could specifically target TLR7, we tested its TLR selectivity. HEK293 cells were co-transfected with different human TLR genes and a SEAP reporter gene under the control of NF- κ B promoter. The inhibitory activities of **Z9j** were tested using the SEAP assay. These HEK hTLR cells were stimulated with distinct TLR ligands, including Pam3CSK4 for TLR1/2, Pam2CSK4 for TLR2/6, poly I:C for TLR3, LPS for TLR4, flagellin for TLR5, R848 for TLR7 and TLR8,

1
2
3 and CpG-ODN2006 for TLR9. As shown in **Figure 2A**, **Z9j** inhibited the SEAP signals
4 triggered by different TLR ligands in a similar manner. To rule out toxicity, the cell viability was
5 evaluated with a colorimetric WST-1 assay. Compound **Z9j** showed negligible cytotoxicity
6 within the concentrations tested (**Figure 2B**). Cumulatively, the results suggested that **Z9j** may
7 target signaling molecules downstream of all these homologous TLRs.
8
9

10
11 To confirm our hypothesis, we examined whether **Z9j** could inhibit NF- κ B signaling through
12 other membrane receptors, such as TNFR and IL-1R (**Figure 2C**). HEK-Blue Null cells were
13 transfected with the SEAP reporter gene under the control of the NF- κ B promoter in the absence
14 of TLRs. Results showed that compound **Z9j** dose-dependently inhibited the SEAP signals
15 stimulated by TNF- α (**Figure 2D**) and IL-1 β (**Figure 2E**) in the transfected HEK-Blue Null
16 cells. Moreover, **Z9j** showed similar IC₅₀ values in both cases: $0.77 \pm 0.04 \mu\text{M}$ for TNF- α
17 stimulation and $0.72 \pm 0.03 \mu\text{M}$ for IL-1 β stimulation. These results clearly pointed to the
18 possibility that **Z9j** targets common downstream pathways shared by all these membrane
19 receptors.
20
21

22
23 NF- κ B signaling can also be activated through upstream cytoplasmic kinases including
24 protein kinase C (PKC).³⁵ To exclude the possibility that membrane receptors are not the target
25 of compound **Z9j**, we examined its effects on NF- κ B signaling activated by phorbol 12-myristate
26 13-acetate (PMA), a known PKC agonist (**Figure 2C**). Indeed, PMA treatment induced strong
27 NF- κ B activation in either HEK hTLR7 (**Figures 2F**) or HEK Null cells (**Figures 2G**) as shown
28 by the SEAP assay. When treated with compound **Z9j**, the PMA-induced NF- κ B activation was
29 dose-dependently inhibited in a similar manner in both HEK hTLR7 (IC₅₀ = $0.59 \pm 0.02 \mu\text{M}$) and
30 HEK Null (IC₅₀ = $0.37 \pm 0.03 \mu\text{M}$) cells. These data further confirmed that **Z9j** did not target
31 membrane receptors.
32
33
34
35
36
37
38
39
40
41
42
43
44
45
46
47
48
49
50
51
52
53
54
55
56
57
58
59
60

1
2
3 Additionally, we examined the inhibitory effect of **Z9j** on NF- κ B signaling in mouse cells.
4
5 NF- κ B activation leads to production of NO by inducible nitric oxide synthase (iNOS) (**Figure**
6
7 **2C**). The levels of NO production can be measured by the 2,3-diaminonaphthalene (DAN) assay.
8
9 Results showed that **Z9j** inhibited the NF- κ B-mediated NO production triggered by either
10
11 interferon (IFN)- γ ($IC_{50} = 0.079 \pm 0.005 \mu M$, **Figure 2H**) or LPS ($0.08 \pm 0.01 \mu M$, **Figure 4B**) in
12
13 a similar manner in mouse macrophage RAW 264.7 cells. These data indicated that the inhibition
14
15 of **Z9j** on NF- κ B signaling worked in both human and mouse cell lines, though their potency
16
17 may differ to a certain extent.
18
19

20
21 On the basis of these cellular results, we moved on to explore the molecular mechanism by
22
23 which **Z9j** inhibited NF- κ B signaling. After LPS stimulation in RAW 264.7 cells, three key
24
25 regulatory pathways are activated including IKK/I κ B pathway, phosphatidylinositol-3-kinase
26
27 (PI3K)/Akt pathway, and mitogen-activated protein kinase (MAPK) signaling pathway.³⁶ The
28
29 changes of the key regulators in these pathways were investigated by Western blotting.
30
31

32
33 Since the phosphorylation of I κ B and its upstream regulator IKK complex are the critical
34
35 steps for activation of NF- κ B signaling, we first measured the effects of **Z9j** on the LPS-initiated
36
37 IKK/I κ B pathway. As shown in **Figure 3A**, LPS significantly stimulated the phosphorylation of
38
39 both IKK $\alpha\beta$ and I κ B α at 15 and 30 minutes. Upon pre-treatment of **Z9j**, the phosphorylation
40
41 levels of IKK $\alpha\beta$ and subsequent I κ B α were decreased at both time intervals. These results
42
43 showed that **Z9j** could inhibit NF- κ B activation via the classical IKK/I κ B cascade.
44
45

46
47 We then looked into the upstream signaling events for IKK/I κ B activation. PI3K and its
48
49 downstream target Akt are upstream regulators of IKK/I κ B signaling in various cells.³⁷⁻³⁹ Thus,
50
51 the effects of **Z9j** on the LPS-induced phosphorylation of PI3K and Akt were examined. LPS
52
53 induced the phosphorylation of both PI3K and Akt in macrophages (**Figure 3B**) and the
54
55

induction was markedly attenuated by **Z9j**, indicating that **Z9j** can inhibit NF- κ B activation via the PI3K/Akt pathway.

MAPKs are well-known signaling adaptors involved in the LPS-induced macrophages.⁴⁰ To determine whether **Z9j** could affect the MAPK pathways, phosphorylation levels of c-Jun N-terminal kinase (JNK), p38, and extracellular signal regulated protein kinase (ERK) were assessed. LPS treatment alone induced phosphorylation of the three major families of MAPKs at both 15 and 30 min (**Figure 3C**). However, **Z9j** showed no or negligible inhibition on the phosphorylation levels of these MAPK isoforms. It has been reported that, once activated, the MAPKs translocate to the nucleus to phosphorylate and thereby transcriptionally activate activator protein 1 (AP-1).^{41, 42} Our results suggested that **Z9j** did not inhibit NF- κ B activation via the MAPK signaling pathway.

Then we turned to search for signaling enzymes upstream of PI3K/Akt. Activation of Src and subsequent spleen tyrosine kinase (Syk) is an early event required for activation of PI3K signaling.^{43, 44} We thus investigated the effect of **Z9j** on levels of phosphorylated Syk and Src in LPS-induced RAW 264.7 cells. As shown in **Figure 3D**, LPS induced increased levels of phosphorylation of both Src and Syk in RAW 264.7 cells. More importantly, **Z9j** could block the phosphorylation of both Src and subsequent Syk in a dose-dependent manner at 30 minutes. We further performed the Src kinase assay in vitro and found **Z9j** could only suppress less than 50% of the Src kinase activity at 5 μ M (**Figure 3E**). The inhibition of the Src kinase activity by **Z9j** is not comparable to the cell-based activity, suggesting that there are probably other novel mechanisms of actions involved.

To further examine whether **Z9j** could directly bind to any of the Src family kinases, we sought to kinase profiling using KINOMEScan™ service (Eurofins DiscoverX) which tested

compound-kinase interactions for dissociation constants (K_{ds}) based on DNA labeled kinases and qPCR readout. As the first attempt, we screened for 15 Src family kinases (BLK, BMX, BTK, FGR, FYN, HCK, ITK, LCK, LYN, SRC, SYK, TEC, TXK, YES1, ZAP70) with **Z9j** at 10 μ M. Results showed that **Z9j** only slightly inhibited Src (75%) and there was no inhibition against Syk (**Figure S2**). Therefore, we increased the concentration of **Z9j** to 20 μ M and expanded the screen to all the kinases involved in the above three regulatory pathways of NF- κ B signaling. The second round of kinase profiling comprised 40 targets, including Src family kinases, PI3Ks, AKTs, MAPKs, and IKKs. It turned out that **Z9j** exhibited only mild inhibition against Erk8 (44%) at 20 μ M (**Figure S3**). Given that **Z9j** did not significantly inhibit most of these kinases in the kinase-profiling assays, there are probably other novel mechanisms of actions of **Z9j** involved, such interfering protein-protein interactions.

Based on these results, we proposed a putative mechanism for **Z9j** inhibition on NF- κ B signaling (**Figure 4**). Briefly, **Z9j** might inhibit NF- κ B signaling by suppressing the Src/Syk, PI3K/Akt and IKK/I κ B pathways, eventually leading to downregulation of inflammatory mediators, whereas with negligible impact on the MAPK pathways. Due to the complexity of NF- κ B signaling and its crosstalk with other signaling pathways, further studies are needed to determine if **Z9j** may also modulate other enzyme molecules or directly target certain protein-protein interactions thereby influencing NF- κ B signaling pathways.^{45, 46}

Therapeutic Potential of Z9j. Aside from looking at the possible mechanism of action of **Z9j**, we further investigated its therapeutic potential. Excessive activation NF- κ B signaling has been implicated in many diseases.¹¹⁻¹⁴ Particularly, inhibitors of NF- κ B signaling have been recognized as potential therapeutic agents against many inflammatory diseases and cancers.¹⁶⁻²² We thus studied the anti-inflammatory and anti-cancer properties of **Z9j**.

The anti-inflammatory potential of compound **Z9j** was investigated in LPS-stimulated RAW 264.7 cells, an extensively used model to study inflammation. The effect of **Z9j** on the production of TNF- α , a well-known inflammatory marker, was tested by enzyme-linked immunosorbent assay (ELISA). As shown in **Figure 5A**, LPS stimulation led to significant production of TNF- α , an indication of a strong inflammatory response. The TNF- α production was efficiently suppressed by **Z9j** in a dose-dependent manner. Another well-recognized inflammatory marker is NO produced by iNOS after activation of NF- κ B (**Figure 2C**). As shown in **Figure 5B**, compound **Z9j** also diminished the NO levels dose-dependently in LPS-stimulated RAW 264.7 cells with an IC₅₀ value of 0.08 ± 0.01 μ M. These experiments demonstrated that **Z9j** could effectively reduce or prevent NF- κ B mediated inflammation, suggesting its potential to be further developed as an anti-inflammatory agent against many inflammatory diseases.

We also investigated whether the inhibition of NF- κ B by **Z9j** has anti-cancer effects in human cancer cells. Cervical cancer HeLa cells were selected as a test system in this study. The antiproliferative effect of **Z9j** on HeLa cells was first examined by the WST-1 assay. As shown in **Figure 5C**, **Z9j** drastically inhibited the growth of HeLa cells in a concentration- and time-dependent manner, with a GI₅₀ (growth inhibition of 50%) value around 1.35 ± 0.08 μ M following exposure to **Z9j** for 48 hours. As a comparison, **Z9j** only showed mild cytotoxicity to the normal human mammary epithelial cells (HuMECs). To further explore the mechanism behind its antiproliferative effect, **Z9j** was subjected to an apoptosis induction assay. The HeLa cancer cells were treated with different concentrations of **Z9j** for 24 hours before flow cytometry analysis by double staining with Annexin V-FITC and propidium iodide (PI). The cells in quadrant Q4 represent living cells, Q3 early apoptotic cells, Q2 late apoptotic cells, and Q1 necrotic cells (**Figure 6A**). Results showed that **Z9j** displayed evident induction of apoptosis in

HeLa cells in a dose-dependent manner compared to the control group (**Figure 6B**), suggesting that the antiproliferative activity of **Z9j** against HeLa cells may result from its ability to induce apoptosis. The effect of **Z9j** on the cell cycle distribution of HeLa cells was also examined by staining cells with propidium iodide and analyzing the percentages of G0/G1, S, and G2/M cell populations with flow cytometry. As shown in **Figures 6C and 6D**, treatment with **Z9j** caused a dose-dependent accumulation of HeLa cells at the G0/G1 phase, along with a decreased population of G2/M phase cells. Collectively, these results suggested that compound **Z9j** may also be developed as an anti-cancer agent.

Taken together, these data suggested that **Z9j** may be further developed as a multifunctional therapeutic agent to treat inflammatory diseases as well as cancers.

CONCLUSION

NF- κ B plays an essential role in regulating a number of cellular activities, thus its aberrant activation contributes to pathogenesis of numerous diseases, such as arthritis, asthma, Alzheimer's disease, sclerosis, sepsis, cardiovascular diseases, diabetes, inflammatory diseases, and many types of cancers. Developing novel small-molecule agents that inhibit NF- κ B signaling would provide potential therapeutics for the treatment of many diseases as well as valuable tools for biological studies. We in this study utilized the strategy of cell-based high-throughput screening to discover novel inhibitors of NF- κ B signaling via the TLR7 pathway. Structural modification and SAR studies of two hit compounds led to successful discovery of the best compound **Z9j** with an over 170-fold of enhanced NF- κ B inhibitory activity. Mechanistic studies using both cellular and molecular approaches revealed that **Z9j** inhibited NF- κ B signaling by suppressing Src/Syk, PI3K/Akt and IKK/I κ B pathways. Moreover, preliminary therapeutic studies showed that **Z9j** effectively inhibited NF- κ B-associated inflammatory

responses in macrophage cells, as well as caused cell growth inhibition, apoptosis induction, and cell cycle arrest in human cervical cancer cells. We obtained herein a novel NF- κ B inhibitor with great potential for further development as multifunctional therapeutic agent to treat inflammatory diseases as well as cancer. Our work has also showcased the efficiency of the cell-based HTS strategy to discover novel therapeutic agents.

EXPERIMENTAL SECTION

General Chemistry Methods. Reagents were purchased from commercial sources and used as received. ^1H NMR spectra were recorded at 400 MHz in $\text{DMSO-}d_6$ using a residual solvent peak (2.50 ppm) as the internal standard. ^{13}C NMR spectra were recorded at 101 MHz in $\text{DMSO-}d_6$ using residual DMSO (39.52 ppm) as the internal reference. Compounds were purified using flash chromatography (ACI systems, Biotage). Purities of all tested compounds were tested using ^1H NMR, ^{13}C NMR, and high-performance liquid chromatography (HPLC) analysis. NMR and HPLC analysis showed that all tested compounds have >95% purity. Mass spectrometry was performed at the mass spectrometry facility of the Department of Chemistry at the University of Colorado at Boulder on a double focusing high-resolution mass spectrometer.

General Procedure for the Preparation of Compounds S3a-k, S10a-l, and S11a-h Exemplified by 3-Amino-N'-(3-(trifluoromethyl)benzoyl)pyrazine-2-carbohydrazide (S3a). *O*-benzotriazol-1-yl-*N,N,N',N'*-tetramethyluronium tetrafluoroborate (TBTU, 346 mg, 1.08 mmol) and triethylamine (0.30 mL, 2.16 mmol) were added to a solution of 3-aminopyrazine-2-carboxylic acid (100 mg, 0.72 mmol) and 3-(trifluoromethyl)benzene-1-carbohydrazide (176 mg, 0.86 mmol) in dimethylformamide (DMF, 10 mL) and the resulting solution stirred at room temperature overnight. The reaction mixture was poured into water and extracted with ethyl acetate. The combined organic layers were dried with Na_2SO_4 , filtered, concentrated, and

purified by flash column chromatography to give the title compound **S3a** (213 mg, 91%) as a light-yellow solid. ^1H NMR (400 MHz, $\text{DMSO}-d_6$) δ 10.77 (s, 1H), 10.68 (s, 1H), 8.30 (s, 1H), 8.26 (s, 1H), 8.23 (d, $J = 7.8$ Hz, 1H), 7.99 (d, $J = 7.5$ Hz, 1H), 7.91 (s, 1H), 7.80 (t, $J = 7.6$ Hz, 1H), 7.54 (br s, 2H); ^{13}C NMR (101 MHz, $\text{DMSO}-d_6$) δ 165.71, 164.63, 155.59, 147.94, 133.84, 132.06, 131.67, 130.42, 129.76 (q, $J = 32.1$ Hz), 128.94 (q, $J = 3.9$ Hz), 125.01, 124.50 (q, $J = 3.9$ Hz), 124.35 (q, $J = 272.4$ Hz); HRMS (ESI^+), calcd $\text{C}_{13}\text{H}_{11}\text{F}_3\text{N}_5\text{O}_2$ ($\text{M} + \text{H}^+$) = 326.0865, found = 326.0862.

3-Amino-N'-(2-(trifluoromethyl)benzoyl)pyrazine-2-carbohydrazide (S3b). Light-yellow solid, yield 92%. ^1H NMR (400 MHz, $\text{DMSO}-d_6$) δ 10.60 (s, 1H), 10.49 (s, 1H), 8.29 (d, $J = 2.3$ Hz, 1H), 7.90 (d, $J = 2.3$ Hz, 1H), 7.86 – 7.79 (m, 2H), 7.74 – 7.69 (m, 2H), 7.53 (br s, 2H); ^{13}C NMR (101 MHz, $\text{DMSO}-d_6$) δ 166.57, 165.52, 155.55, 147.89, 134.54 (d, $J = 2.3$ Hz), 132.90, 131.64, 130.96, 129.72, 127.34 (q, $J = 31.7$ Hz), 126.89 (d, $J = 4.6$ Hz), 125.06, 121.28 (d, $J = 273.8$ Hz); HRMS (ESI^+), calcd $\text{C}_{13}\text{H}_{11}\text{F}_3\text{N}_5\text{O}_2$ ($\text{M} + \text{H}^+$) = 326.0865, found = 326.0861.

3-Amino-N'-(4-(trifluoromethyl)benzoyl)pyrazine-2-carbohydrazide (S3c). Yellow solid, yield 89%. ^1H NMR (400 MHz, $\text{DMSO}-d_6$) δ 10.69 (br s, 2H), 8.29 (d, $J = 1.8$ Hz, 1H), 8.11 (d, $J = 8.1$ Hz, 2H), 7.93 (s, 1H), 7.90 (d, $J = 2.3$ Hz, 2H), 7.53 (br s, 2H); ^{13}C NMR (101 MHz, $\text{DMSO}-d_6$) δ 165.46, 164.86, 155.60, 147.86, 137.09, 131.99 (d, $J = 31.5$ Hz), 131.67, 128.84, 125.99 (q, $J = 3.6$ Hz), 125.72, 125.17, 121.66 (d, $J = 272.3$ Hz); HRMS (ESI^+), calcd $\text{C}_{13}\text{H}_{11}\text{F}_3\text{N}_5\text{O}_2$ ($\text{M} + \text{H}^+$) = 326.0865, found = 326.0867.

3-Amino-N'-(3-(trifluoromethyl)benzoyl)picolinohydrazide (S3d). White solid, yield 90%. ^1H NMR (400 MHz, $\text{DMSO}-d_6$) δ 10.70 (s, 1H), 10.39 (s, 1H), 8.26 (s, 0H), 8.22 (d, $J = 7.7$ Hz, 0H), 7.99 (d, $J = 7.7$ Hz, 0H), 7.86 (dd, $J = 4.2, 1.4$ Hz, 1H), 7.79 (t, $J = 7.8$ Hz, 0H), 7.31 (dd, $J = 8.5, 4.2$ Hz, 1H), 7.22 (dd, $J = 8.5, 1.5$ Hz, 1H), 6.83 (s, 2H). ^{13}C NMR (101 MHz, $\text{DMSO}-d_6$)

δ 166.98, 164.59, 147.06, 136.30, 134.01, 132.06, 130.37, 129.72 (q, $J = 32.2$ Hz), 128.84 (q, $J = 3.7$ Hz), 128.23, 128.05, 125.06, 124.51 (q, $J = 3.8$ Hz), 124.39 (q, $J = 272.5$ Hz); HRMS (ESI⁺), calcd C₁₄H₁₂F₃N₄O₂ (M + H⁺) = 325.0912, found = 325.0912.

N'-(3-(trifluoromethyl)benzoyl)pyrazine-2-carbohydrazide (S3e). Light-yellow solid, yield 95%. ¹H NMR (400 MHz, DMSO-*d*₆) δ 10.97 (s, 2H), 9.23 (s, 1H), 8.95 (s, 1H), 8.82 (s, 1H), 8.27 – 8.23 (m, 2H), 8.00 (d, $J = 7.3$ Hz, 1H), 7.81 (t, $J = 7.5$ Hz, 1H); ¹³C NMR (101 MHz, DMSO-*d*₆) δ 164.53, 162.71, 148.55, 144.59, 144.21, 144.12, 133.81, 132.08, 130.44, 129.62 (q, $J = 32.2$ Hz), 128.97 (q, $J = 3.7$ Hz), 124.51 (q, $J = 4.0$ Hz), 124.36 (q, $J = 272.5$ Hz); HRMS (ESI⁺), calcd C₁₃H₁₀F₃N₄O₂ (M + H⁺) = 311.0756, found = 311.0755.

2-Amino-N'-(3-(trifluoromethyl)benzoyl)nicotinohydrazide (S3f). White solid, yield 98%. ¹H NMR (400 MHz, DMSO-*d*₆) δ 10.76 (s, 1H), 10.53 (s, 1H), 8.26 – 8.23 (m, 2H), 8.16 (d, $J = 3.5$ Hz, 1H), 8.04 – 8.00 (m, 2H), 7.81 (t, $J = 7.8$ Hz, 1H), 7.08 (s, 2H), 6.65 (dd, $J = 7.7, 4.8$ Hz, 1H); ¹³C NMR (101 MHz, DMSO-*d*₆) δ 167.57, 165.04, 159.26, 152.61, 137.12, 133.77, 132.04, 130.48, 129.82 (q, $J = 32.1$ Hz), 129.02 (q, $J = 3.6$ Hz), 124.48 (q, $J = 3.8$ Hz), 124.35 (q, $J = 272.5$ Hz), 111.87, 107.82; HRMS (ESI⁺), calcd C₁₄H₁₂F₃N₄O₂ (M + H⁺) = 325.0912, found = 325.0916.

3-Chloro-N'-(3-(trifluoromethyl)benzoyl)pyrazine-2-carbohydrazide (S3g). Yellow solid, yield 97%. ¹H NMR (400 MHz, DMSO-*d*₆) δ 11.00 (s, 2H), 8.80 (d, $J = 2.4$ Hz, 1H), 8.73 (d, $J = 2.4$ Hz, 1H), 8.29 (s, 1H), 8.25 (d, $J = 7.9$ Hz, 1H), 8.01 (d, $J = 7.9$ Hz, 1H), 7.81 (t, $J = 7.8$ Hz, 1H); ¹³C NMR (101 MHz, DMSO-*d*₆) δ 164.34, 162.90, 146.78, 146.47, 146.03, 143.06, 133.59, 132.14, 130.45, 129.79 (d, $J = 32.2$ Hz), 129.05 (q, $J = 3.4$ Hz), 124.57 (q, $J = 3.6$ Hz), 124.36 (d, $J = 272.6$ Hz); HRMS (ESI⁺), calcd C₁₃H₉ClF₃N₄O₂ (M + H⁺) = 345.0366, found = 345.0363.

3-Hydroxy-N'-(3-(trifluoromethyl)benzoyl)picolinohydrazide (S3h). White solid, yield 93%. ^1H NMR (400 MHz, $\text{DMSO-}d_6$) δ 11.85 (br s, 1H), 11.15 (br s, 2H), 8.26 – 8.22 (m, 3H), 8.00 (d, $J = 7.8$ Hz, 1H), 7.81 (t, $J = 7.8$ Hz, 1H), 7.61 (dd, $J = 8.5, 4.3$ Hz, 1H), 7.49 (dd, $J = 8.5, 1.2$ Hz, 1H); ^{13}C NMR (101 MHz, $\text{DMSO-}d_6$) δ 168.23, 164.47, 157.68, 140.67, 133.67, 132.09, 131.04, 130.47, 130.04, 129.80 (q, $J = 32.2$ Hz), 129.04 (d, $J = 3.5$ Hz), 126.57, 124.51 (q, $J = 3.7$ Hz), 124.34 (q, $J = 272.5$ Hz); HRMS (ESI^+), calcd $\text{C}_{14}\text{H}_{11}\text{F}_3\text{N}_3\text{O}_3$ ($\text{M} + \text{H}^+$) = 326.0753, found = 326.0748.

N'-(3-(trifluoromethyl)benzoyl)picolinohydrazide (S3i). White solid, yield 99%. ^1H NMR (400 MHz, $\text{DMSO-}d_6$) δ 10.87 (s, 1H), 10.79 (s, 1H), 8.72 (ddd, $J = 4.8, 1.6, 1.0$ Hz, 1H), 8.27 (s, 1H), 8.24 (d, $J = 7.9$ Hz, 1H), 8.10 – 8.03 (m, 2H), 8.00 (d, $J = 7.8$ Hz, 1H), 7.80 (t, $J = 7.8$ Hz, 1H), 7.68 (ddd, $J = 6.9, 4.8, 1.9$ Hz, 1H); ^{13}C NMR (101 MHz, $\text{DMSO-}d_6$) δ 164.49, 163.69, 149.57, 149.18, 138.36, 133.84, 132.08, 130.42, 129.76 (q, $J = 32.1$ Hz), 128.94 (q, $J = 3.4$ Hz), 127.56, 124.52 (q, $J = 3.8$ Hz), 124.37 (q, $J = 272.5$ Hz), 122.90; HRMS (ESI^+), calcd $\text{C}_{14}\text{H}_{11}\text{F}_3\text{N}_3\text{O}_2$ ($\text{M} + \text{H}^+$) = 310.0803, found = 310.0802.

3-Amino-6-bromo-N'-(3-(trifluoromethyl)benzoyl)pyrazine-2-carbohydrazide (S3j). Yellow solid, yield 99%. ^1H NMR (400 MHz, $\text{DMSO-}d_6$) δ 10.77 (s, 1H), 10.63 (s, 1H), 8.44 (s, 1H), 8.24 – 8.21 (m, 2H), 8.00 (d, $J = 7.8$ Hz, 1H), 7.80 (t, $J = 7.8$ Hz, 1H), 7.69 (s, 2H); ^{13}C NMR (101 MHz, $\text{DMSO-}d_6$) δ 164.73, 164.71, 154.64, 150.05, 133.80, 132.08, 130.46, 129.78 (q, $J = 32.2$ Hz), 128.99 (d, $J = 3.7$ Hz), 124.48 (q, $J = 4.2$ Hz), 124.35 (q, $J = 272.5$ Hz), 122.24; HRMS (ESI^+), calcd $\text{C}_{13}\text{H}_{10}\text{BrF}_3\text{N}_5\text{O}_2$ ($\text{M} + \text{H}^+$) = 403.9970, found = 403.9966.

3-Amino-6-chloro-N'-(3-(trifluoromethyl)benzoyl)pyrazine-2-carbohydrazide (S3k). Light-yellow solid, yield 94%. ^1H NMR (400 MHz, $\text{DMSO-}d_6$) δ 10.78 (s, 1H), 10.64 (s, 1H), 8.41 (s, 1H), 8.25 – 8.21 (m, 2H), 8.00 (d, $J = 7.8$ Hz, 1H), 7.80 (t, $J = 7.8$ Hz, 1H), 7.69 (s, 2H);

¹³C NMR (101 MHz, DMSO-*d*₆) δ 164.73, 164.68, 154.47, 147.50, 133.80, 132.38, 132.08, 130.45, 129.78 (q, *J* = 32.1 Hz), 128.98 (q, *J* = 3.5 Hz), 124.48 (q, *J* = 3.8 Hz), 124.35 (q, *J* = 272.5 Hz), 123.09; HRMS (ESI⁺), calcd C₁₃H₁₀ClF₃N₅O₂ (M + H⁺) = 360.0475, found = 360.0475.

Synthesis of N-(4-oxo-2-propyl-1,4-dihydropteridin-3(2H)-yl)-3-(trifluoromethyl)benzamide (S4). A mixture of 3-amino-*N'*-(3-(trifluoromethyl)benzoyl)pyrazine-2-carbohydrazide **S3a** (100 mg, 0.31 mmol), butyraldehyde **S5** (0.054 mL, 0.61 mmol) and a catalytic amount of *p*-toluenesulfonic acid monohydrate in dioxane (10 mL) was refluxed for 2 h. The reaction mixture was concentrated and extracted with ethyl acetate. The combined organic layers were dried with Na₂SO₄, filtered, concentrated, and purified by flash column chromatography to give the title compound **S4** (57 mg, 49%) as a light-yellow solid. ¹H NMR (400 MHz, DMSO-*d*₆) δ 11.19 (s, 1H), 8.41 (d, *J* = 2.6 Hz, 1H), 8.27 – 8.22 (m, 3H), 8.04 – 8.02 (m, 2H), 7.82 (t, *J* = 7.8 Hz, 1H), 5.13 (q, *J* = 5.0, 4.2 Hz, 1H), 1.82 – 1.77 (m, 2H), 1.54–1.30 (m, 2H), 0.87 (t, *J* = 7.3 Hz, 3H); ¹³C NMR (101 MHz, DMSO-*d*₆) δ 164.60, 160.16, 154.40, 147.70, 135.20, 133.30, 132.35, 130.50, 129.78 (q, *J* = 32.2 Hz), 129.30 (q, *J* = 3.3 Hz), 126.65, 124.68 (q, *J* = 3.8 Hz), 124.32 (q, *J* = 272.5 Hz), 70.99, 36.61, 16.71, 14.15; HRMS (ESI⁺), calcd C₁₇H₁₇F₃N₅O₂ (M + H⁺) = 380.1334, found = 380.1333.

Preparation of N-hexyl-4-(hydrazinecarbonyl)benzamide (S7I). A mixture of 4-(hexylcarbamoyl)benzoic acid **S9I** (300 mg, 1.20 mmol), hydrazine (0.38 mL, 12.03 mmol), HOBt (163 mg, 1.20 mmol), and EDCI (277 mg, 1.44 mmol) in DMF (20 mL) and stirred at room temperature overnight. The reaction mixture was poured into water and extracted with ethyl acetate. The combined organic layers were dried with Na₂SO₄, filtered, concentrated, and purified by flash column chromatography to give the title compound **S7I** (291 mg, 92%) as a

white solid. ^1H NMR (400 MHz, $\text{DMSO}-d_6$) δ 9.91 (s, 1H), 8.56 (s, 1H), 7.88 (s, 4H), 4.56 (br s, 2H), 3.31 – 3.19 (m, 2H), 1.52 (m, 2H), 1.36 – 1.22 (m, 6H), 0.87 (t, J = 8.0 Hz, 3H); MS (ESI^+) m/z 264.2 $[\text{M}+\text{H}]^+$.

Preparation of 4-(hexylcarbamoyl)benzoic acid (S9I). 1-(3-Dimethylaminopropyl)-3-ethylcarbodiimide hydrochloride (EDCI, 415 mg, 2.17 mmol) and *N,N*-diisopropylethylamine (DIPEA, 0.75 mL, 4.51 mmol) were added to a solution of terephthalic acid **S8** (300 mg, 1.81 mmol), hexylamine (0.24 mL, 1.81 mmol) and 1-hydroxybenzotriazole (HOBt, 293 mg, 2.17 mmol) in DMF (20 mL) and stirred at room temperature overnight. The reaction mixture was poured into water and extracted with ethyl acetate. The combined organic layers were dried with Na_2SO_4 , filtered, concentrated, and purified by flash column chromatography to give the title compound **S9I** (427 mg, 95%) as a white solid. ^1H NMR (400 MHz, $\text{DMSO}-d_6$) δ 13.46 (br s, 1H), 8.62 (t, J = 5.6 Hz, 1H), 8.03 – 7.98 (m, 2H), 7.95 – 7.90 (m, 2H), 3.26 (td, J = 7.1, 5.6 Hz, 2H), 1.57 – 1.45 (m, 2H), 1.35 – 1.22 (m, 6H), 0.86 (t, J = 8.0 Hz, 3H); MS (ESI^+) m/z 250.1 $[\text{M}+\text{H}]^+$.

3-Amino-*N'*-(4-chlorobenzoyl)pyrazine-2-carbohydrazide (S10a). Yellow solid, yield 87%. ^1H NMR (400 MHz, $\text{DMSO}-d_6$) δ 10.58 – 10.56 (m, 2H), 8.29 (d, J = 1.9 Hz, 1H), 7.95 – 7.90 (m, 3H), 7.61 (d, J = 8.4 Hz, 2H), 7.51 (br s, 2H); ^{13}C NMR (101 MHz, DMSO) δ 165.72, 165.01, 155.57, 147.88, 137.14, 131.74, 131.65, 129.85, 129.10, 125.10; HRMS (ESI^+), calcd $\text{C}_{12}\text{H}_{11}\text{ClN}_5\text{O}_2$ ($\text{M} + \text{H}^+$) = 292.0601, found = 292.0608.

3-Amino-*N'*-(4-bromobenzoyl)pyrazine-2-carbohydrazide (S10b). Yellow solid, yield 86%. ^1H NMR (400 MHz, $\text{DMSO}-d_6$) δ 10.59 – 10.57 (m, 2H), 8.28 (d, J = 2.1 Hz, 1H), 7.90 – 7.85 (m, 3H), 7.75 (d, J = 8.4 Hz, 2H), 7.51 (br s, 2H); ^{13}C NMR (101 MHz, DMSO) δ 165.71,

165.16, 155.57, 147.89, 132.09, 132.04, 131.66, 130.03, 126.11, 125.08; HRMS (ESI⁺), calcd C₁₂H₁₁BrN₅O₂ (M + H⁺) = 336.0096, found = 336.0101.

3-Amino-N'-(2,6-dichlorobenzoyl)pyrazine-2-carbohydrazide (S10c). Light-yellow solid, yield 93%. ¹H NMR (400 MHz, DMSO-*d*₆) δ 10.78 (s, 1H), 10.64 (s, 1H), 8.29 (d, *J* = 2.3 Hz, 1H), 7.90 (d, *J* = 2.3 Hz, 1H), 7.56 – 7.47 (m, 5H); ¹³C NMR (101 MHz, DMSO) δ 165.03, 162.72, 155.53, 147.89, 134.99, 132.33, 132.08, 131.61, 128.65, 125.03; HRMS (ESI⁺), calcd C₁₂H₁₀Cl₂N₅O₂ (M + H⁺) = 326.0212, found = 326.0212.

3-Amino-N'-(2-chloro-4-nitrobenzoyl)pyrazine-2-carbohydrazide (S10d). Yellow solid, yield 82%. ¹H NMR (400 MHz, DMSO-*d*₆) δ 10.72 – 10.69 (m, 2H), 8.40 – 8.29 (m, 3H), 7.90 (d, *J* = 2.2 Hz, 1H), 7.80 (d, *J* = 8.4 Hz, 1H), 7.53 (br s, 2H); ¹³C NMR (101 MHz, DMSO) δ 165.46, 164.50, 155.57, 149.12, 148.01, 140.76, 132.11, 131.70, 131.04, 125.27, 124.85, 122.90; HRMS (ESI⁺), calcd C₁₂H₁₀ClN₆O₄ (M + H⁺) = 337.0452, found = 337.0450.

3-Amino-N'-(2,4-difluorobenzoyl)pyrazine-2-carbohydrazide (S10e). Yellow solid, yield 99%. ¹H NMR (400 MHz, DMSO-*d*₆) δ 10.61 (s, 1H), 10.32 (s, 1H), 8.28 (d, *J* = 2.3 Hz, 1H), 7.89 (d, *J* = 2.3 Hz, 1H), 7.74 (q, *J* = 8.2 Hz, 1H), 7.52 – 7.39 (m, 3H), 7.24 (td, *J* = 8.5, 2.0 Hz, 1H); ¹³C NMR (101 MHz, DMSO-*d*₆) δ 165.48, 164.19 (d, *J* = 238.6 Hz), 162.85 (d, *J* = 2.1 Hz), 160.42 (dd, *J* = 253.8, 12.8 Hz), 155.57, 147.90, 132.44 (d, *J* = 10.5 Hz), 131.66, 125.02, 119.37 (d, *J* = 18.4 Hz), 112.39 (d, *J* = 25.2 Hz), 105.31 (t, *J* = 26.2 Hz); HRMS (ESI⁺), calcd C₁₂H₁₀F₂N₅O₂ (M + H⁺) = 294.0803, found = 294.0803.

3-Amino-N'-(4-cyanobenzoyl)pyrazine-2-carbohydrazide (S10f). Light-yellow solid, yield 90%. ¹H NMR (400 MHz, DMSO-*d*₆) δ 10.75 (s, 1H), 10.67 (s, 1H), 8.29 (d, *J* = 2.3 Hz, 1H), 8.07 – 8.04 (m, 4H), 7.90 (d, *J* = 2.3 Hz, 1H), 7.53 (br s, 2H); ¹³C NMR (101 MHz, DMSO) δ

165.70, 164.70, 155.58, 147.96, 136.94, 133.12, 131.68, 128.75, 124.97, 118.69, 114.69; HRMS (ESI⁺), calcd C₁₃H₁₁N₆O₂ (M + H⁺) = 283.0943, found = 283.0943.

3-Amino-N'-(4-methoxybenzoyl)pyrazine-2-carbohydrazide (S10g). Yellow solid, yield 99%. ¹H NMR (400 MHz, DMSO-*d*₆) δ 10.48 (s, 1H), 10.32 (s, 1H), 8.28 (d, *J* = 2.3 Hz, 1H), 8.00 – 7.75 (m, 3H), 7.50 (br s, 2H), 7.05 (d, *J* = 8.8 Hz, 2H), 3.84 (s, 3H); ¹³C NMR (101 MHz, DMSO) δ 165.78, 165.53, 162.45, 155.55, 147.78, 131.64, 129.84, 125.28, 125.13, 114.15, 55.86; HRMS (ESI⁺), calcd C₁₃H₁₄N₅O₃ (M + H⁺) = 288.1097, found = 288.1095.

3-Amino-N'-(4-hydroxybenzoyl)pyrazine-2-carbohydrazide (S10h). Yellow solid, yield 72%. ¹H NMR (400 MHz, DMSO-*d*₆) δ 10.44 (s, 1H), 10.20 (s, 1H), 10.13 (s, 1H), 8.28 (s, 1H), 7.89 (s, 1H), 7.79 (d, *J* = 8.4 Hz, 2H), 7.51 (br s, 2H), 6.85 (d, *J* = 8.4 Hz, 2H); ¹³C NMR (101 MHz, DMSO) δ 165.77, 165.70, 161.08, 155.54, 147.75, 131.61, 129.96, 125.33, 123.59, 115.43; HRMS (ESI⁺), calcd C₁₂H₁₂N₅O₃ (M + H⁺) = 274.0940, found = 274.0943.

3-Amino-N'-(4-(trifluoromethoxy)benzoyl)pyrazine-2-carbohydrazide (S10i). Yellow solid, yield 95%. ¹H NMR (400 MHz, DMSO-*d*₆) δ 10.62 (s, 2H), 8.29 (d, *J* = 2.3 Hz, 1H), 8.04 (d, *J* = 8.8 Hz, 2H), 7.90 (d, *J* = 2.3 Hz, 1H), 7.55-7.53 (m, 4H); ¹³C NMR (101 MHz, DMSO-*d*₆) δ 165.72, 164.85, 155.58, 151.12 (q, *J* = 1.7 Hz), 147.90, 132.07, 131.66, 130.32, 125.07, 121.28, 120.42 (d, *J* = 257.3 Hz); HRMS (ESI⁺), calcd C₁₃H₁₁F₃N₅O₃ (M + H⁺) = 342.0814, found = 342.0814.

Methyl 4-(2-(3-aminopyrazine-2-carbonyl)hydrazine-1-carbonyl)benzoate (S10j). Yellow solid, yield 70%. ¹H NMR (400 MHz, DMSO-*d*₆) δ 10.67 (s, 1H), 10.64 (s, 1H), 8.29 (d, *J* = 2.2 Hz, 1H), 8.10 (d, *J* = 8.3 Hz, 2H), 8.03 (d, *J* = 8.4 Hz, 2H), 7.90 (d, *J* = 2.2 Hz, 1H), 7.53 (br s, 2H), 3.90 (s, 3H); ¹³C NMR (101 MHz, DMSO) δ 166.10, 165.70, 165.27, 155.58, 147.92,

137.10, 132.77, 131.66, 129.77, 128.37, 125.05, 52.91; HRMS (ESI⁺), calcd C₁₄H₁₄N₅O₄ (M + H⁺) = 316.1046, found = 316.1046.

3-Amino-N'-nicotinoylpyrazine-2-carbohydrazide (S10k). White solid, yield 90%. ¹H NMR (400 MHz, DMSO-*d*₆) δ 10.70-10.66 (m, 2H), 9.07 (dd, *J* = 2.2, 0.8 Hz, 1H), 8.78 (dd, *J* = 4.8, 1.7 Hz, 1H), 8.29 (d, *J* = 2.3 Hz, 1H), 8.26 (ddd, *J* = 8.0, 2.3, 1.7 Hz, 1H), 7.90 (d, *J* = 2.3 Hz, 1H), 7.60 – 7.53 (m, 3H); ¹³C NMR (101 MHz, DMSO) δ 165.73, 164.65, 155.58, 152.98, 148.90, 147.95, 135.69, 131.68, 128.65, 125.00, 124.16; HRMS (ESI⁺), calcd C₁₁H₁₁N₆O₂ (M + H⁺) = 259.0943, found = 259.0939.

4-(2-(3-Aminopyrazine-2-carbonyl)hydrazine-1-carbonyl)-N-hexylbenzamide (S10l). Light-yellow solid, yield 78% from compound **S8**. ¹H NMR (400 MHz, DMSO-*d*₆) δ 10.61-10.58 (m, 2H), 8.62 (t, *J* = 5.6 Hz, 1H), 8.29 (d, *J* = 2.3 Hz, 1H), 8.00 – 7.94 (m, 4H), 7.90 (d, *J* = 2.2 Hz, 1H), 7.52 (br s, 2H), 3.27 (q, *J* = 8.2, 7.4 Hz, 2H), 1.55 – 1.52 (m, 2H), 1.30 (s, 6H), 0.88 (t, *J* = 6.5 Hz, 3H); ¹³C NMR (101 MHz, DMSO) δ 165.78, 165.72, 165.43, 155.58, 147.89, 137.97, 135.04, 131.66, 127.90, 127.73, 125.11, 31.49, 29.47, 26.64, 22.53, 14.40; HRMS (ESI⁺), calcd C₁₉H₂₅N₆O₃ (M + H⁺) = 385.1988, found = 385.1989.

N'-(4-(trifluoromethoxy)benzoyl)picolinohydrazide (S11a). White solid, yield 99%. ¹H NMR (400 MHz, DMSO-*d*₆) δ 10.73 (s, 1H), 10.70 (s, 1H), 8.72 (d, *J* = 4.6 Hz, 1H), 8.08 – 8.03 (m, 4H), 7.70 – 7.66 (m, 1H), 7.54 (d, *J* = 8.2 Hz, 2H); ¹³C NMR (101 MHz, DMSO-*d*₆) δ 164.72, 163.71, 151.12 (d, *J* = 1.9 Hz), 149.63, 149.17, 138.35, 132.08, 130.34, 127.53, 122.88, 121.27, 120.42 (q, *J* = 257.2 Hz); HRMS (ESI⁺), calcd C₁₄H₁₁F₃N₃O₃ (M + H⁺) = 326.0753, found = 326.0753.

N'-(4-(trifluoromethyl)benzoyl)picolinohydrazide (S11b). White solid, yield 97%. ¹H NMR (400 MHz, DMSO-*d*₆) δ 10.84 (s, 1H), 10.78 (s, 1H), 8.72 (d, *J* = 4.5 Hz, 1H), 8.14 – 8.03 (m,

4H), 7.93 (d, $J = 8.1$ Hz, 2H), 7.68 (ddd, $J = 6.9, 4.8, 1.8$ Hz, 1H); ^{13}C NMR (101 MHz, DMSO- d_6) δ 164.83, 163.69, 149.59, 149.17, 138.34, 136.80 (d, $J = 1.5$ Hz), 132.13 (q, $J = 31.9$ Hz), 128.89, 127.54, 126.02 (q, $J = 3.7$ Hz), 124.32 (q, $J = 272.6$ Hz), 122.89; HRMS (ESI $^+$), calcd $\text{C}_{14}\text{H}_{11}\text{F}_3\text{N}_3\text{O}_2$ ($\text{M} + \text{H}^+$) = 310.0803, found = 310.0806.

N'-(4-bromobenzoyl)picolinohydrazide (S11c). White solid, yield 97%. ^1H NMR (400 MHz, DMSO- d_6) δ 10.71 (s, 1H), 10.67 (s, 1H), 8.72 – 8.71 (m, 1H), 8.09 – 8.02 (m, 2H), 7.88 (d, $J = 8.5$ Hz, 2H), 7.76 (d, $J = 8.6$ Hz, 2H), 7.67 (ddd, $J = 6.9, 4.8, 2.1$ Hz, 1H); ^{13}C NMR (101 MHz, DMSO) δ 165.03, 163.69, 149.64, 149.16, 138.35, 132.10, 132.04, 130.05, 127.52, 126.12, 122.87; HRMS (ESI $^+$), calcd $\text{C}_{13}\text{H}_{11}\text{BrN}_3\text{O}_2$ ($\text{M} + \text{H}^+$) = 320.0035, found = 320.0038.

N'-(4-chlorobenzoyl)picolinohydrazide (S11d). White solid, yield 91%. ^1H NMR (400 MHz, DMSO- d_6) δ 10.69 (s, 1H), 10.66 (s, 1H), 8.72 – 8.71 (m, 1H), 8.09 – 8.03 (m, 2H), 7.95 (d, $J = 8.6$ Hz, 2H), 7.67 (ddd, $J = 6.9, 4.8, 2.2$ Hz, 1H), 7.62 (d, $J = 8.6$ Hz, 2H); ^{13}C NMR (101 MHz, DMSO) δ 164.91, 163.71, 149.64, 149.16, 138.34, 137.15, 131.74, 129.88, 129.09, 127.51, 122.87; HRMS (ESI $^+$), calcd $\text{C}_{13}\text{H}_{11}\text{ClN}_3\text{O}_2$ ($\text{M} + \text{H}^+$) = 276.0540, found = 276.0544.

3-Hydroxy-N'-(4-(trifluoromethoxy)benzoyl)picolinohydrazide (S11e). White solid, yield 99%. ^1H NMR (400 MHz, DMSO- d_6) δ 11.90 – 10.75 (m, 3H), 8.24 (d, $J = 4.2$ Hz, 1H), 8.06 (d, $J = 8.3$ Hz, 2H), 7.62 – 7.48 (m, 4H); ^{13}C NMR (101 MHz, DMSO- d_6) δ 168.31, 164.69, 157.69, 151.20, 140.64, 131.85, 131.07, 130.37, 130.01, 126.55, 121.30, 120.41 (q, $J = 257.3$ Hz); HRMS (ESI $^+$), calcd $\text{C}_{14}\text{H}_{11}\text{F}_3\text{N}_3\text{O}_4$ ($\text{M} + \text{H}^+$) = 342.0702, found = 342.0704.

3-Hydroxy-N'-(4-(trifluoromethyl)benzoyl)picolinohydrazide (S11f). Light-yellow solid, yield 83%. ^1H NMR (400 MHz, DMSO- d_6) δ 11.90 – 11.15 (m, 3H), 8.25 (s, 1H), 8.13 (d, $J = 7.3$ Hz, 2H), 7.94 (d, $J = 7.8$ Hz, 2H), 7.60 (s, 1H), 7.50 (d, $J = 8.8$ Hz, 1H); ^{13}C NMR (101 MHz, DMSO- d_6) δ 168.22, 164.75, 157.69, 140.65, 136.61, 132.20 (q, $J = 31.0$ Hz), 131.07,

130.02, 128.90, 126.57, 126.08 (d, $J = 3.5$ Hz), 124.32 (q, $J = 272.5$ Hz); HRMS (ESI⁺), calcd C₁₄H₁₁F₃N₃O₃ (M + H⁺) = 326.0753, found = 326.0760.

N'-(4-bromobenzoyl)-3-hydroxypicolinohydrazide (S11g). Light-yellow solid, yield 87%. ¹H NMR (400 MHz, DMSO-*d*₆) δ 11.14 (br s, 3H), 8.23 (d, $J = 3.4$ Hz, 1H), 7.87 (d, $J = 8.2$ Hz, 2H), 7.76 (d, $J = 8.1$ Hz, 2H), 7.59 (dd, $J = 7.8, 4.1$ Hz, 1H), 7.48 (d, $J = 8.3$ Hz, 1H); ¹³C NMR (101 MHz, DMSO) δ 168.20, 164.94, 157.74, 140.57, 132.70, 132.08, 131.97, 130.05, 127.51, 126.55, 126.20; HRMS (ESI⁺), calcd C₁₃H₁₁BrN₃O₃ (M + H⁺) = 335.9984, found = 335.9985.

N'-(4-chlorobenzoyl)-3-hydroxypicolinohydrazide (S11h). Light-yellow solid, yield 82%. ¹H NMR (400 MHz, DMSO-*d*₆) δ 11.87 – 11.06 (m, 3H), 8.24 (dd, $J = 4.4, 1.4$ Hz, 1H), 7.95 (d, $J = 8.6$ Hz, 2H), 7.64 – 7.59 (m, 3H), 7.49 (dd, $J = 8.5, 1.4$ Hz, 1H); ¹³C NMR (101 MHz, DMSO) δ 168.29, 164.85, 157.69, 140.64, 137.27, 131.53, 131.08, 130.01, 129.89, 129.16, 126.55; HRMS (ESI⁺), calcd C₁₃H₁₁ClN₃O₃ (M + H⁺) = 292.0489, found = 292.0490.

General Procedure for the Preparation of Compounds Z3a-f, Z5a-n, Z7a-d, and Z9a-o Exemplified by N'-(4-chlorobenzoyl)-2-methylthiazole-4-carbohydrazide (Z3a). *O*-benzotriazol-1-yl-*N,N,N'*-tetramethyluronium tetrafluoroborate (TBTU, 336 mg, 1.05 mmol) and triethylamine (0.30 mL, 2.10 mmol) were added to a solution of 2-methyl-1,3-thiazole-4-carboxylic acid (100 mg, 0.70 mmol) and 4-chlorobenzene-1-carbohydrazide (143 mg, 0.84 mmol) in DMF (10 mL) and the resulting solution stirred at room temperature overnight. The reaction mixture was poured into water and extracted with ethyl acetate. The combined organic layers were dried with Na₂SO₄, filtered, concentrated, and purified by flash column chromatography to give the title compound **Z3a** (196 mg, 95%) as a white solid. ¹H NMR (400 MHz, DMSO-*d*₆) δ 10.61 (s, 1H), 10.33 (s, 1H), 8.25 (s, 1H), 7.94 (d, $J = 8.5$ Hz, 2H), 7.61 (d, $J = 8.6$ Hz, 2H), 2.75 (s, 3H); ¹³C NMR (101 MHz, DMSO) δ 166.97, 164.90, 160.33, 148.22,

137.13, 131.73, 129.88, 129.07, 125.55, 19.28; HRMS (ESI⁺), calcd C₁₂H₁₁ClN₃O₂S (M + H⁺) = 296.0261, found = 296.0268.

N'-(4-chlorobenzoyl)-2-methylthiazole-5-carbohydrazide (Z3b). White solid, yield 96%. ¹H NMR (400 MHz, DMSO-*d*₆) δ 10.69 (s, 1H), 10.67 (s, 1H), 8.33 (s, 1H), 7.93 (d, *J* = 8.5 Hz, 2H), 7.62 (d, *J* = 8.5 Hz, 2H), 2.72 (s, 3H); ¹³C NMR (101 MHz, DMSO) δ 170.93, 165.34, 160.09, 144.13, 137.32, 132.78, 131.49, 129.83, 129.18, 19.67; HRMS (ESI⁺), calcd C₁₂H₁₁ClN₃O₂S (M + H⁺) = 296.0261, found = 296.0267.

N'-(4-chlorobenzoyl)thiazole-2-carbohydrazide (Z3c). White solid, yield 73%. ¹H NMR (400 MHz, DMSO-*d*₆) δ 10.86 (s, 1H), 10.73 (s, 1H), 8.15 (d, *J* = 3.0 Hz, 1H), 8.11 (d, *J* = 3.0 Hz, 1H), 7.93 (d, *J* = 8.5 Hz, 2H), 7.62 (d, *J* = 8.5 Hz, 2H); ¹³C NMR (101 MHz, DMSO) δ 164.98, 162.26, 159.12, 144.76, 137.28, 131.51, 129.87, 129.16, 126.68; HRMS (ESI⁺), calcd C₁₁H₉ClN₃O₂S (M + H⁺) = 282.0104, found = 282.0109.

N'-(4-chlorobenzoyl)-1H-indole-2-carbohydrazide (Z3d). White solid, yield 80%. ¹H NMR (400 MHz, DMSO-*d*₆) δ 11.75 (s, 1H), 10.65 (s, 1H), 10.58 (s, 1H), 7.97 (d, *J* = 8.5 Hz, 2H), 7.68-7.63 (m, 3H), 7.47 (d, *J* = 8.2 Hz, 1H), 7.28 (s, 1H), 7.23 (t, *J* = 7.6 Hz, 1H), 7.08 (t, *J* = 7.5 Hz, 1H); ¹³C NMR (101 MHz, DMSO) δ 165.37, 161.26, 137.26, 137.11, 131.68, 129.91, 129.86, 129.18, 127.44, 124.21, 122.22, 120.41, 112.85, 103.95; HRMS (ESI⁺), calcd C₁₆H₁₃ClN₃O₂ (M + H⁺) = 314.0696, found = 314.0705.

3-Chloro-N'-(4-chlorobenzoyl)-6-methylbenzo[*b*]thiophene-2-carbohydrazide (Z3e). White solid, yield 97%. ¹H NMR (400 MHz, DMSO-*d*₆) δ 10.78 (s, 1H), 10.52 (s, 1H), 7.97 – 7.94 (m, 3H), 7.82 (d, *J* = 8.3 Hz, 1H), 7.63 (d, *J* = 8.5 Hz, 2H), 7.44 (d, *J* = 8.3 Hz, 1H), 2.49 (s, 3H); ¹³C NMR (101 MHz, DMSO) δ 164.99, 160.56, 138.45, 137.60, 137.34, 134.28, 131.49,

129.88, 129.18, 128.46, 128.29, 123.38, 122.85, 121.24, 21.70; HRMS (ESI⁺), calcd C₁₇H₁₃Cl₂N₂O₂S (M + H⁺) = 379.0075, found = 379.0075.

N'-(4-chlorobenzoyl)-3-isopropyl-1H-pyrazole-5-carbohydrazide (Z3f). *Light-yellow* solid, yield 92%. ¹H NMR (400 MHz, DMSO-*d*₆) δ 13.11 (s, 1H), 10.50 (s, 1H), 10.05 (s, 1H), 7.93 (d, *J* = 8.5 Hz, 2H), 7.60 (d, *J* = 8.5 Hz, 2H), 6.49 (s, 1H), 2.99 (dq, *J* = 11.2, 5.8, 4.6 Hz, 1H), 1.25 (d, *J* = 6.9 Hz, 6H); ¹³C NMR (101 MHz, DMSO) δ 165.09, 161.86, 151.22, 145.35, 137.05, 131.86, 129.84, 129.05, 102.38, 25.54, 22.76; HRMS (ESI⁺), calcd C₁₄H₁₆ClN₄O₂ (M + H⁺) = 307.0962, found = 307.0966.

N'-(2-chlorobenzoyl)-2-methylthiazole-4-carbohydrazide (Z5a). White solid, yield 94%. ¹H NMR (400 MHz, DMSO-*d*₆) δ 10.44 (s, 1H), 10.34 (s, 1H), 8.25 (s, 1H), 7.57 – 7.43 (m, 4H), 2.75 (s, 3H); ¹³C NMR (101 MHz, DMSO) δ 166.90, 165.76, 160.06, 148.17, 135.02, 131.93, 131.00, 130.36, 129.93, 127.54, 125.52, 19.28; HRMS (ESI⁺), calcd C₁₂H₁₁ClN₃O₂S (M + H⁺) = 296.0261, found = 296.0266.

N'-(3-chlorobenzoyl)-2-methylthiazole-4-carbohydrazide (Z5b). White solid, yield 90%. ¹H NMR (400 MHz, DMSO-*d*₆) δ 10.65 (s, 1H), 10.36 (s, 1H), 8.25 (s, 1H), 7.95 (t, *J* = 1.9 Hz, 1H), 7.88 (d, *J* = 7.8 Hz, 1H), 7.70 – 7.67 (m, 1H), 7.57 (t, *J* = 7.9 Hz, 1H), 2.75 (s, 3H); ¹³C NMR (101 MHz, DMSO) δ 166.99, 164.53, 160.29, 148.17, 134.93, 133.78, 132.17, 131.04, 127.74, 126.69, 125.61, 19.28; HRMS (ESI⁺), calcd C₁₂H₁₁ClN₃O₂S (M + H⁺) = 296.0261, found = 296.0264.

N'-(3-cyanobenzoyl)-2-methylthiazole-4-carbohydrazide (Z5c). White solid, yield 99%. ¹H NMR (400 MHz, DMSO-*d*₆) δ 10.76 (s, 1H), 10.43 (s, 1H), 8.31 (s, 1H), 8.26 (s, 1H), 8.22 (d, *J* = 8.0 Hz, 1H), 8.09 (d, *J* = 7.7 Hz, 1H), 7.76 (t, *J* = 7.8 Hz, 1H), 2.75 (s, 3H); ¹³C NMR (101 MHz, DMSO) δ 167.04, 164.13, 160.28, 148.08, 135.81, 133.95, 132.66, 131.54, 130.49, 125.72,

1
2
3 118.64, 112.20, 19.28; HRMS (ESI⁺), calcd C₁₃H₁₁N₄O₂S (M + H⁺) = 287.0603, found =
4
5 287.0605.
6

7 **Methyl 3-(2-(2-methylthiazole-4-carbonyl)hydrazine-1-carbonyl)benzoate (Z5d).** White
8 solid, yield 70%. ¹H NMR (400 MHz, DMSO-*d*₆) δ 10.75 (s, 1H), 10.38 (s, 1H), 8.52 (t, *J* = 1.6
9
10 Hz, 1H), 8.26 (s, 1H), 8.17 (dt, *J* = 7.9, 1.6 Hz, 2H), 7.70 (t, *J* = 7.8 Hz, 1H), 3.91 (s, 3H), 2.76
11
12 (s, 3H); ¹³C NMR (101 MHz, DMSO) δ 166.99, 166.15, 165.05, 160.29, 148.20, 133.54, 132.73,
13
14 132.56, 130.39, 129.68, 128.72, 125.62, 52.89, 19.29; HRMS (ESI⁺), calcd C₁₄H₁₄N₃O₄S (M +
15
16 H⁺) = 320.0705, found = 320.0705.
17
18
19

20 **N'-(3-fluorobenzoyl)-2-methylthiazole-4-carbohydrazide (Z5e).** White solid, yield 97%. ¹H
21 NMR (400 MHz, DMSO-*d*₆) δ 10.63 (s, 1H), 10.37 (s, 1H), 8.26 (s, 1H), 7.78 (d, *J* = 7.8 Hz,
22
23 1H), 7.70 (d, *J* = 9.7 Hz, 1H), 7.59 (td, *J* = 7.9, 6.0 Hz, 1H), 7.47 (td, *J* = 8.4, 2.0 Hz, 1H), 2.75
24
25 (s, 3H); ¹³C NMR (101 MHz, DMSO-*d*₆) δ 166.99, 164.56 (d, *J* = 2.5 Hz), 162.39 (d, *J* = 244.6
26
27 Hz), 160.34, 148.18, 135.22 (d, *J* = 6.9 Hz), 131.23 (d, *J* = 7.9 Hz), 125.62, 124.15 (d, *J* = 2.8
28
29 Hz), 119.27 (d, *J* = 21.0 Hz), 114.71 (d, *J* = 23.0 Hz), 19.28; HRMS (ESI⁺), calcd C₁₂H₁₁FN₃O₂S
30
31 (M + H⁺) = 280.0556, found = 280.0558.
32
33
34
35
36

37 **N'-(3-bromobenzoyl)-2-methylthiazole-4-carbohydrazide (Z5f).** Light-yellow solid, yield
38 99%. ¹H NMR (400 MHz, DMSO-*d*₆) δ 10.65 (s, 1H), 10.37 (s, 1H), 8.25 (s, 1H), 8.09 (t, *J* = 1.8
39
40 Hz, 1H), 7.93 – 7.90 (m, 1H), 7.83-7.80 (m, 1H), 7.51 (t, *J* = 7.9 Hz, 1H), 2.75 (s, 3H); ¹³C NMR
41
42 (101 MHz, DMSO) δ 166.99, 164.44, 160.29, 148.16, 135.09, 135.07, 131.29, 130.61, 127.06,
43
44 125.64, 122.22, 19.29; HRMS (ESI⁺), calcd C₁₂H₁₁BrN₃O₂S (M + H⁺) = 339.9755, found =
45
46 339.9757.
47
48
49
50

51 **N'-(3-hydroxybenzoyl)-2-methylthiazole-4-carbohydrazide (Z5g).** White solid, yield 75%.
52 ¹H NMR (400 MHz, DMSO-*d*₆) δ 10.40 (s, 1H), 10.25 (s, 1H), 9.76 (s, 1H), 8.24 (s, 1H), 7.93 –
53
54
55
56
57
58
59
60

7.28 (m, 3H), 6.97 (d, $J = 7.6$ Hz, 1H), 2.74 (s, 3H); ^{13}C NMR (101 MHz, DMSO) δ 166.90, 165.95, 160.34, 157.81, 148.33, 134.41, 129.93, 125.43, 119.16, 118.41, 114.94, 19.29; HRMS (ESI^+), calcd $\text{C}_{12}\text{H}_{12}\text{N}_3\text{O}_3\text{S}$ ($\text{M} + \text{H}^+$) = 278.0599, found = 278.0605.

2-Methyl-N'-(3-(trifluoromethyl)benzoyl)thiazole-4-carbohydrazide (Z5h). White solid, yield 98%. ^1H NMR (400 MHz, $\text{DMSO}-d_6$) δ 10.80 (s, 1H), 10.40 (s, 1H), 8.27 – 8.21 (m, 3H), 8.00 (d, $J = 7.8$ Hz, 1H), 7.80 (t, $J = 7.8$ Hz, 1H), 2.76 (s, 3H); ^{13}C NMR (101 MHz, $\text{DMSO}-d_6$) δ 167.02, 164.48, 160.29, 148.14, 133.85, 132.08, 130.41, 129.75 (q, $J = 32.1$ Hz), 128.92 (d, $J = 3.6$ Hz), 125.65, 124.51 (q, $J = 4.0$ Hz), 124.37 (q, $J = 272.8$ Hz), 19.28; HRMS (ESI^+), calcd $\text{C}_{13}\text{H}_{11}\text{F}_3\text{N}_3\text{O}_2\text{S}$ ($\text{M} + \text{H}^+$) = 330.0524, found = 330.0527.

N'-(3,5-dichlorobenzoyl)-2-methylthiazole-4-carbohydrazide (Z5i). White solid, yield 91%. ^1H NMR (400 MHz, $\text{DMSO}-d_6$) δ 10.76 (s, 1H), 10.44 (s, 1H), 8.27 (s, 1H), 7.93 (d, $J = 1.9$ Hz, 2H), 7.91 (t, $J = 1.9$ Hz, 1H), 2.75 (s, 3H); ^{13}C NMR (101 MHz, DMSO) δ 167.04, 163.24, 160.22, 148.03, 136.03, 134.97, 131.81, 126.74, 125.77, 19.28. HRMS (ESI^+), calcd $\text{C}_{12}\text{H}_{10}\text{Cl}_2\text{N}_3\text{O}_2\text{S}$ ($\text{M} + \text{H}^+$) = 329.9871, found = 329.9876.

2-Methyl-N'-(3-(trifluoromethoxy)benzoyl)thiazole-4-carbohydrazide (Z5j). White solid, yield 99%. ^1H NMR (400 MHz, $\text{DMSO}-d_6$) δ 10.75 (s, 1H), 10.41 (s, 1H), 8.27 (s, 1H), 7.98 (d, $J = 7.3$ Hz, 1H), 7.87 (s, 1H), 7.71 – 7.62 (m, 2H), 2.75 (s, 3H); ^{13}C NMR (101 MHz, $\text{DMSO}-d_6$) δ 166.98, 164.36 (d, $J = 4.1$ Hz), 160.30, 148.83, 148.21 (d, $J = 4.4$ Hz), 135.17, 131.23, 127.02 (d, $J = 4.9$ Hz), 125.48, 124.79, 120.54 (q, $J = 257.6$ Hz), 120.36, 19.24; HRMS (ESI^+), calcd $\text{C}_{13}\text{H}_{11}\text{F}_3\text{N}_3\text{O}_3\text{S}$ ($\text{M} + \text{H}^+$) = 346.0473, found = 346.0472.

N'-(3-methoxybenzoyl)-2-methylthiazole-4-carbohydrazide (Z5k). White solid, yield 88%. ^1H NMR (400 MHz, $\text{DMSO}-d_6$) δ 10.50 (s, 1H), 10.31 (s, 1H), 8.24 (s, 1H), 7.51 – 7.41 (m, 3H), 7.16 (ddd, $J = 8.1, 2.7, 1.1$ Hz, 1H), 3.83 (s, 3H), 2.75 (s, 3H); ^{13}C NMR (101 MHz, DMSO) δ

166.96, 165.58, 160.34, 159.64, 148.32, 134.37, 130.10, 125.50, 120.22, 118.22, 112.94, 55.77, 19.30; HRMS (ESI⁺), calcd C₁₃H₁₄N₃O₃S (M + H⁺) = 292.0756, found = 292.0759.

2-Methyl-N'-picolinoylthiazole-4-carbohydrazide (Z5l). White solid, yield 98%. ¹H NMR (400 MHz, DMSO-*d*₆) δ 10.61 (s, 1H), 10.32 (s, 1H), 8.71 – 8.69 (m, 1H), 8.24 (s, 1H), 8.07 – 8.01 (m, 2H), 7.66 (ddd, *J* = 6.5, 4.7, 2.5 Hz, 1H), 2.74 (s, 3H); ¹³C NMR (101 MHz, DMSO) δ 166.87, 163.41, 160.06, 149.70, 149.09, 148.31, 138.30, 127.45, 125.46, 122.85, 19.28; HRMS (ESI⁺), calcd C₁₁H₁₁N₄O₂S (M + H⁺) = 263.0603, found = 263.0603.

2-Methyl-N'-nicotinoylthiazole-4-carbohydrazide (Z5m). White solid, yield 88%. ¹H NMR (400 MHz, DMSO-*d*₆) δ 10.74 (s, 1H), 10.41 (s, 1H), 9.06 (dd, *J* = 2.3, 0.9 Hz, 1H), 8.78 (dd, *J* = 4.8, 1.7 Hz, 1H), 8.27 – 8.24 (m, 2H), 7.57 (ddd, *J* = 8.0, 4.8, 0.9 Hz, 1H), 2.75 (s, 3H); ¹³C NMR (101 MHz, DMSO) δ 167.02, 164.51, 160.29, 152.94, 148.93, 148.14, 135.70, 128.65, 125.67, 124.14, 19.30; HRMS (ESI⁺), calcd C₁₁H₁₁N₄O₂S (M + H⁺) = 263.0603, found = 263.0601.

N'-isonicotinoyl-2-methylthiazole-4-carbohydrazide (Z5n). White solid, yield 90%. ¹H NMR (400 MHz, DMSO-*d*₆) δ 10.84 (s, 1H), 10.46 (s, 1H), 8.80 – 8.78 (m, 2H), 8.27 (s, 1H), 7.83 – 7.81 (m, 2H), 2.75 (s, 3H); ¹³C NMR (101 MHz, DMSO) δ 167.07, 164.40, 160.28, 150.93, 148.08, 139.94, 125.78, 121.82, 19.29; HRMS (ESI⁺), calcd C₁₁H₁₁N₄O₂S (M + H⁺) = 263.0603, found = 263.0608.

2-Isopropyl-N'-picolinoylthiazole-4-carbohydrazide (Z7a). White solid, yield 92%. ¹H NMR (400 MHz, DMSO-*d*₆) δ 10.66 (s, 1H), 10.29 (s, 1H), 8.70 (d, *J* = 4.8 Hz, 1H), 8.28 (s, 1H), 8.08 – 8.02 (m, 2H), 7.66 (t, *J* = 5.8 Hz, 1H), 3.37 – 3.25 (m, 1H), 1.39 (d, *J* = 6.8 Hz, 6H); ¹³C NMR (101 MHz, DMSO) δ 178.12, 163.51, 160.16, 149.69, 149.08, 148.12, 138.29, 127.46,

124.50, 122.86, 33.05, 23.20; HRMS (ESI⁺), calcd C₁₃H₁₅N₄O₂S (M + H⁺) = 291.0916, found = 291.0914.

2-Phenyl-N'-picolinoylthiazole-4-carbohydrazide (Z7b). White solid, yield 99%. ¹H NMR (400 MHz, DMSO-*d*₆) δ 10.76 (s, 1H), 10.59 (s, 1H), 8.72 (d, *J* = 4.7 Hz, 1H), 8.46 (s, 1H), 8.14 – 8.03 (m, 4H), 7.69 – 7.66 (m, 1H), 7.57 – 7.55 (m, 3H); ¹³C NMR (101 MHz, DMSO) δ 167.91, 163.65, 160.05, 149.71, 149.39, 149.14, 138.33, 132.89, 131.31, 129.73, 127.50, 127.00, 125.72, 122.92; HRMS (ESI⁺), calcd C₁₆H₁₃N₄O₂S (M + H⁺) = 325.0759, found = 325.0759.

N'-picolinoyl-2-(pyridin-4-yl)thiazole-4-carbohydrazide (Z7c). White solid, yield 72%. ¹H NMR (400 MHz, DMSO-*d*₆) δ 10.78 (s, 1H), 10.67 (s, 1H), 8.80 – 8.78 (m, 2H), 8.74 – 8.72 (m, 1H), 8.61 (s, 1H), 8.10 – 8.04 (m, 4H), 7.69 (ddd, *J* = 6.9, 4.8, 1.9 Hz, 1H); ¹³C NMR (101 MHz, DMSO) δ 165.31, 163.67, 159.79, 151.27, 149.80, 149.67, 149.16, 139.45, 138.36, 127.68, 127.53, 122.93, 120.80; HRMS (ESI⁺), calcd C₁₅H₁₂N₅O₂S (M + H⁺) = 326.0712, found = 326.0720.

N'-picolinoyl-2-(pyridin-3-yl)thiazole-4-carbohydrazide (Z7d). White solid, yield 81%. ¹H NMR (400 MHz, DMSO-*d*₆) δ 10.77 (s, 1H), 10.64 (s, 1H), 9.35 (s, 1H), 8.74 – 8.72 (m, 2H), 8.54 (s, 1H), 8.48 (dt, *J* = 8.1, 1.9 Hz, 1H), 8.10 – 8.03 (m, 2H), 7.69 (ddd, *J* = 7.0, 4.8, 1.9 Hz, 1H), 7.61 (dd, *J* = 8.0, 4.8 Hz, 1H); ¹³C NMR (101 MHz, DMSO) δ 164.97, 163.68, 159.89, 151.86, 149.71, 149.53, 149.17, 147.82, 138.37, 134.46, 128.89, 127.54, 126.58, 124.71, 122.94; HRMS (ESI⁺), calcd C₁₅H₁₂N₅O₂S (M + H⁺) = 326.0712, found = 326.0722.

2-(4-Fluorophenyl)-N'-picolinoylthiazole-4-carbohydrazide (Z9a). White solid, yield 90%. ¹H NMR (400 MHz, DMSO-*d*₆) δ 10.75 (s, 1H), 10.60 (s, 1H), 8.72 (d, *J* = 4.7 Hz, 1H), 8.45 (s, 1H), 8.21 – 8.03 (m, 4H), 7.68 (t, *J* = 5.9 Hz, 1H), 7.42 (t, *J* = 8.6 Hz, 2H); ¹³C NMR (101 MHz, DMSO-*d*₆) δ 166.71, 164.01 (d, *J* = 248.7 Hz), 163.65, 159.99, 149.70, 149.33, 149.13, 138.33,

129.59 (d, $J = 3.0$ Hz), 129.39 (d, $J = 8.7$ Hz), 127.50, 125.78, 122.91, 116.79 (d, $J = 22.1$ Hz);
HRMS (ESI⁺), calcd C₁₆H₁₂FN₄O₂S (M + H⁺) = 343.0665, found = 343.0671.

2-(4-Chlorophenyl)-N'-picolinoylthiazole-4-carbohydrazide (Z9b). White solid, yield 74%.
¹H NMR (400 MHz, DMSO-*d*₆) δ 10.76 (s, 1H), 10.62 (s, 1H), 8.72 (ddd, $J = 4.7, 1.7, 1.0$ Hz, 1H), 8.48 (s, 1H), 8.17 – 8.13 (m, 2H), 8.10 – 8.02 (m, 2H), 7.69 – 7.61 (m, 3H); ¹³C NMR (101 MHz, DMSO) δ 166.54, 163.64, 159.95, 149.70, 149.44, 149.13, 138.32, 135.89, 131.74, 129.78, 128.71, 127.50, 126.13, 122.91; HRMS (ESI⁺), calcd C₁₆H₁₂ClN₄O₂S (M + H⁺) = 359.0369, found = 359.0374.

N'-picolinoyl-2-(4-(trifluoromethyl)phenyl)thiazole-4-carbohydrazide (Z9c). White solid, yield 95%. ¹H NMR (400 MHz, DMSO-*d*₆) δ 10.77 (s, 1H), 10.67 (s, 1H), 8.74 – 8.72 (m, 1H), 8.56 (s, 1H), 8.36 (d, $J = 8.1$ Hz, 2H), 8.10 – 8.04 (m, 2H), 7.95 (d, $J = 8.2$ Hz, 2H), 7.69 (ddd, $J = 6.9, 4.7, 1.8$ Hz, 1H); ¹³C NMR (101 MHz, DMSO-*d*₆) δ 166.05, 163.65, 159.87, 149.69, 149.15, 138.35, 136.43, 130.93 (q, $J = 31.9$ Hz), 127.73, 127.52, 127.03, 126.72 (q, $J = 3.9$ Hz), 124.43 (q, $J = 272.3$ Hz), 122.92; HRMS (ESI⁺), calcd C₁₇H₁₂F₃N₄O₂S (M + H⁺) = 393.0633, found = 393.0635.

N'-picolinoyl-2-(p-tolyl)thiazole-4-carbohydrazide (Z9d). White solid, yield 91%. ¹H NMR (400 MHz, DMSO-*d*₆) δ 10.74 (s, 1H), 10.56 (s, 1H), 8.72 (d, $J = 4.6$ Hz, 1H), 8.41 (s, 1H), 8.10 – 8.01 (m, 4H), 7.68 (ddd, $J = 7.0, 4.8, 1.6$ Hz, 1H), 7.36 (d, $J = 7.9$ Hz, 2H), 2.38 (s, 3H); ¹³C NMR (101 MHz, DMSO) δ 168.02, 163.62, 160.07, 149.72, 149.27, 149.13, 141.26, 138.33, 130.32, 130.25, 127.49, 126.94, 125.19, 122.90, 21.47; HRMS (ESI⁺), calcd C₁₇H₁₅N₄O₂S (M + H⁺) = 339.0916, found = 339.0923.

2-(4-Ethylphenyl)-N'-picolinoylthiazole-4-carbohydrazide (Z9e). White solid, yield 86%.
¹H NMR (400 MHz, DMSO-*d*₆) δ 10.75 (s, 1H), 10.56 (s, 1H), 8.72 (d, $J = 4.7$ Hz, 1H), 8.41 (s,

1H), 8.10 – 8.03 (m, 4H), 7.68 (t, $J = 6.2$ Hz, 1H), 7.39 (d, $J = 7.9$ Hz, 2H), 2.68 (q, $J = 7.9$ Hz, 2H), 1.22 (t, $J = 7.5$ Hz, 3H); ^{13}C NMR (101 MHz, DMSO) δ 168.03, 163.63, 160.07, 149.72, 149.29, 149.13, 147.42, 138.33, 130.57, 129.09, 127.50, 127.05, 125.24, 122.91, 28.53, 15.75; HRMS (ESI⁺), calcd C₁₈H₁₇N₄O₂S (M + H⁺) = 353.1072, found = 353.1079.

2-(4-Methoxyphenyl)-N'-picolinoylthiazole-4-carbohydrazide (Z9f). White solid, yield 99%. ^1H NMR (400 MHz, DMSO- d_6) δ 10.73 (s, 1H), 10.52 (s, 1H), 8.73 (ddd, $J = 4.8, 1.6, 1.0$ Hz, 1H), 8.35 (s, 1H), 8.10 – 8.03 (m, 4H), 7.68 (ddd, $J = 7.2, 4.8, 1.8$ Hz, 1H), 7.13 – 7.09 (m, 2H), 3.85 (s, 3H); ^{13}C NMR (101 MHz, DMSO) δ 167.81, 163.63, 161.78, 160.09, 149.72, 149.14, 138.34, 128.66, 127.50, 125.71, 124.65, 122.90, 115.07, 55.94; HRMS (ESI⁺), calcd C₁₇H₁₅N₄O₃S (M + H⁺) = 355.0865, found = 355.0869.

2-(4-(Dimethylamino)phenyl)-N'-picolinoylthiazole-4-carbohydrazide (Z9g). White solid, yield 90%. ^1H NMR (400 MHz, DMSO- d_6) δ 10.70 (s, 1H), 10.44 (s, 1H), 8.73 (dt, $J = 4.7, 1.4$ Hz, 1H), 8.22 (s, 1H), 8.10 – 8.03 (m, 2H), 7.92 (d, $J = 8.9$ Hz, 2H), 7.68 (ddd, $J = 6.9, 4.8, 1.9$ Hz, 1H), 6.81 (d, $J = 9.0$ Hz, 2H), 3.02 (s, 6H); ^{13}C NMR (101 MHz, DMSO) δ 168.79, 163.57, 160.20, 152.29, 149.76, 149.13, 148.96, 138.33, 128.20, 127.47, 123.07, 122.89, 120.55, 112.20, 39.98; HRMS (ESI⁺), calcd C₁₈H₁₈N₅O₂S (M + H⁺) = 368.1181, found = 368.1183.

2-(3,4-Dimethoxyphenyl)-N'-picolinoylthiazole-4-carbohydrazide (Z9h). White solid, yield 92%. ^1H NMR (400 MHz, DMSO- d_6) δ 10.77 (s, 1H), 10.56 (s, 1H), 8.73 (d, $J = 4.4$ Hz, 1H), 8.35 (s, 1H), 8.10 – 8.03 (m, 2H), 7.79 (d, $J = 2.0$ Hz, 1H), 7.68 (ddd, $J = 7.0, 4.7, 1.7$ Hz, 1H), 7.60 (dd, $J = 8.3, 2.1$ Hz, 1H), 7.10 (d, $J = 8.4$ Hz, 1H), 3.90 (s, 3H), 3.85 (s, 3H); ^{13}C NMR (101 MHz, DMSO) δ 167.91, 163.75, 160.07, 151.53, 149.73, 149.56, 149.16, 148.97, 138.36, 127.52, 125.78, 124.70, 122.93, 120.31, 112.27, 109.86, 56.17, 56.15; HRMS (ESI⁺), calcd C₁₈H₁₇N₄O₄S (M + H⁺) = 385.0971, found = 385.0977.

2-(2,3-Dichlorophenyl)-N'-picolinoylthiazole-4-carbohydrazide (Z9i). White solid, yield 85%. ^1H NMR (400 MHz, $\text{DMSO}-d_6$) δ 10.76 (s, 1H), 10.68 (s, 1H), 8.73 (ddd, $J = 4.8, 1.7, 1.0$ Hz, 1H), 8.65 (s, 1H), 8.55 (dd, $J = 8.0, 1.6$ Hz, 1H), 8.10 – 8.03 (m, 2H), 7.85 (dd, $J = 8.0, 1.6$ Hz, 1H), 7.68 (ddd, $J = 7.1, 4.8, 1.9$ Hz, 1H), 7.59 (t, $J = 8.0$ Hz, 1H); ^{13}C NMR (101 MHz, DMSO) δ 163.64, 162.66, 159.92, 149.70, 149.15, 148.32, 138.35, 133.50, 133.38, 132.50, 130.50, 129.65, 129.03, 127.73, 127.51, 122.92; HRMS (ESI^+), calcd $\text{C}_{16}\text{H}_{11}\text{Cl}_2\text{N}_4\text{O}_2\text{S}$ ($\text{M} + \text{H}^+$) = 392.9980, found = 392.9982.

2-(2,4-Dichlorophenyl)-N'-picolinoylthiazole-4-carbohydrazide (Z9j). White solid, yield 81%. ^1H NMR (400 MHz, $\text{DMSO}-d_6$) δ 10.76 (s, 1H), 10.71 (s, 1H), 8.73 (d, $J = 4.8$ Hz, 1H), 8.68 (d, $J = 8.7$ Hz, 1H), 8.61 (s, 1H), 8.10 – 8.03 (m, 2H), 7.89 (d, $J = 2.1$ Hz, 1H), 7.69 – 7.67 (m, 2H); ^{13}C NMR (101 MHz, DMSO) δ 163.64, 162.02, 159.92, 149.71, 149.14, 148.26, 138.33, 135.93, 132.81, 132.21, 130.58, 130.04, 128.49, 127.50, 127.40, 122.91; HRMS (ESI^+), calcd $\text{C}_{16}\text{H}_{11}\text{Cl}_2\text{N}_4\text{O}_2\text{S}$ ($\text{M} + \text{H}^+$) = 392.9980, found = 392.9985.

2-(3,5-Dichlorophenyl)-N'-picolinoylthiazole-4-carbohydrazide (Z9k). White solid, yield 89%. ^1H NMR (400 MHz, $\text{DMSO}-d_6$) δ 10.78 (s, 1H), 10.71 (s, 1H), 8.73 (d, $J = 4.4$ Hz, 1H), 8.55 (s, 1H), 8.25 (d, $J = 1.7$ Hz, 2H), 8.10 – 8.04 (m, 2H), 7.81 (t, $J = 1.9$ Hz, 1H), 7.69 (ddd, $J = 6.9, 4.9, 1.9$ Hz, 1H); ^{13}C NMR (101 MHz, DMSO) δ 164.48, 163.69, 159.76, 149.69, 149.32, 149.16, 138.36, 135.95, 135.53, 130.33, 127.53, 127.24, 125.53, 122.93; HRMS (ESI^+), calcd $\text{C}_{16}\text{H}_{11}\text{Cl}_2\text{N}_4\text{O}_2\text{S}$ ($\text{M} + \text{H}^+$) = 392.9980, found = 392.9981.

2-(3-Fluorophenyl)-N'-picolinoylthiazole-4-carbohydrazide (Z9l). White solid, yield 92%. ^1H NMR (400 MHz, $\text{DMSO}-d_6$) δ 10.77 (s, 1H), 10.65 (s, 1H), 8.73 (ddd, $J = 4.8, 1.7, 1.0$ Hz, 1H), 8.50 (s, 1H), 8.10 – 8.03 (m, 3H), 7.93 (ddd, $J = 7.8, 1.6, 0.9$ Hz, 1H), 7.68 (ddd, $J = 7.2, 4.7, 1.7$ Hz, 1H), 7.61 (td, $J = 8.0, 5.9$ Hz, 1H), 7.43 – 7.37 (m, 1H); ^{13}C NMR (101 MHz,

DMSO-*d*₆) δ 166.25 (d, J = 3.2 Hz), 163.68, 163.01 (d, J = 244.55 Hz), 159.90, 149.70, 149.31, 149.15, 138.35, 135.06 (d, J = 8.4 Hz), 131.95 (d, J = 8.4 Hz), 127.52, 126.40, 123.29 (d, J = 2.8 Hz), 122.92, 118.06 (d, J = 21.3 Hz), 113.52 (d, J = 23.7 Hz); HRMS (ESI⁺), calcd C₁₆H₁₂FN₄O₂S (M + H⁺) = 343.0665, found = 343.0673.

2-(3-Chlorophenyl)-N'-picolinoylthiazole-4-carbohydrazide (Z9m). White solid, yield 88%. ¹H NMR (400 MHz, DMSO-*d*₆) δ 10.76 (s, 1H), 10.66 (s, 1H), 8.73 (dt, J = 4.8, 1.4 Hz, 1H), 8.50 (s, 1H), 8.33 (t, J = 1.9 Hz, 1H), 8.10 – 8.02 (m, 3H), 7.69 (ddd, J = 6.9, 4.8, 1.9 Hz, 1H), 7.64 – 7.57 (m, 2H); ¹³C NMR (101 MHz, DMSO) δ 166.06, 163.65, 159.88, 149.71, 149.37, 149.15, 138.34, 134.75, 134.61, 131.68, 130.95, 127.51, 126.45, 126.40, 125.82, 122.91; HRMS (ESI⁺), calcd C₁₆H₁₂ClN₄O₂S (M + H⁺) = 359.0369, found = 359.0375.

2-(3-Bromophenyl)-N'-picolinoylthiazole-4-carbohydrazide (Z9n). Light-yellow solid, yield 92%. ¹H NMR (400 MHz, DMSO-*d*₆) δ 10.76 (s, 1H), 10.67 (s, 1H), 8.74 – 8.72 (m, 1H), 8.50 (s, 1H), 8.46 (t, J = 1.9 Hz, 1H), 8.10 – 8.03 (m, 3H), 7.74 (ddd, J = 8.0, 2.1, 1.0 Hz, 1H), 7.68 (ddd, J = 6.9, 4.8, 1.7 Hz, 1H), 7.52 (t, J = 7.9 Hz, 1H); ¹³C NMR (101 MHz, DMSO) δ 165.97, 163.67, 159.89, 149.71, 149.38, 149.15, 138.35, 134.91, 133.85, 131.89, 129.19, 127.51, 126.46, 126.20, 123.12, 122.92; HRMS (ESI⁺), calcd C₁₆H₁₂BrN₄O₂S (M + H⁺) = 404.9844, found = 404.9842.

N'-picolinoyl-2-(3-(trifluoromethyl)phenyl)thiazole-4-carbohydrazide (Z9o). White solid, yield 83%. ¹H NMR (400 MHz, DMSO-*d*₆) δ 10.79 (s, 1H), 10.72 (s, 1H), 8.73 (d, J = 4.7 Hz, 1H), 8.59 (s, 1H), 8.54 (s, 1H), 8.35 (d, J = 7.8 Hz, 1H), 8.10 – 8.04 (m, 2H), 7.91 (d, J = 7.8 Hz, 1H), 7.80 (t, J = 7.8 Hz, 1H), 7.68 (ddd, J = 7.0, 4.8, 1.7 Hz, 1H); ¹³C NMR (101 MHz, DMSO-*d*₆) δ 166.01, 163.71, 159.88, 149.71, 149.47, 149.15, 138.35, 133.79, 131.12, 131.01, 130.56 (q,

$J = 32.1$ Hz), 127.54 (d, $J = 4.2$ Hz), 126.66, 124.38 (q, $J = 272.8$ Hz), 123.30 (q, $J = 3.9$ Hz), 122.92; HRMS (ESI⁺), calcd C₁₇H₁₂F₃N₄O₂S (M + H⁺) = 393.0633, found = 393.0633.

Reagents. TLR ligands Pam₃CSK₄, Pam₂CSK₄, poly I:C, LPS, flagellin, R848, CpG-ODN2006, Zeocin, Blastidicin, and QUANTI-Blue were purchased from InvivoGen (San Diego, CA, USA). PMA and WST-1 proliferation reagent were purchased from Sigma-Aldrich (St. Louis, MO, USA). TNF- α ELISA kit and Annexin V-FITC Apoptosis Detection kit were purchased from BD Biosciences (San Jose, CA, USA). Cell Cycle Phase Determination kit was purchased from Cayman Chemical (Ann Arbor, MI, USA). Monoclonal antibodies against IKK β , I κ B α , PI3K, Akt, JNK, p38, ERK, Src, Syk, GAPDH, phospho-IKK $\alpha\beta$ (Ser¹⁷⁶/Ser¹⁷⁷), phospho-I κ B α (Ser³²), phospho-PI3K (Tyr⁴⁵⁸/Tyr¹⁹⁹), phospho-Akt (Ser⁴⁷³), phospho-JNK (Thr¹⁸³/Tyr¹⁸⁵), phospho-p38 (Thr¹⁸⁰/Tyr¹⁸²), phospho-ERK (Thr²⁰²/Tyr²⁰⁴), phospho-Src (Tyr⁴¹⁶), and phospho-Syk (Tyr^{525/526}) were from Cell Signaling Technology (Danvers, MA, USA). Anti-rabbit IgG, HRP-linked secondary antibody was from Jackson ImmunoResearch (West Grove, PA, USA). Nuclear and cytoplasmic extraction reagents, Halt protease inhibitor cocktail, Halt phosphatase inhibitor cocktail, Pierce BCA protein assay kit, heat shock treated BSA, Pierce enhanced chemiluminescence (ECL) Western blot detection reagent, and Restore Western blot stripping buffer were from Thermo Fisher Scientific (Lafayette, CO, USA). ADP-Glo kinase assay kit was from Promega (Madison, WI, USA). Src active kinase (S19-10G) and Src substrate (S30-58) were from SignalChem (Richmond, Canada). All the synthesized small molecules were dissolved in DMSO at 10 mM as a stock solution.

Cell Culture. HEK293 cells stably transfected with human TLR2, TLR3, TLR4, TLR5, TLR7, TLR8, TLR9 and a SEAP reporter gene were obtained from InvivoGen. SEAP expression is maintained by culturing the cells in Dulbecco's modified Eagle's medium (DMEM)

supplemented with 10% fetal bovine serum (FBS) and 1% PenStrep (100 U/mL Penicillin and 100 µg/mL Streptomycin) containing selective antibiotics such as Zeocin and/or Blasticidin according to the manufacturer's instructions. RAW 264.7 cells and HeLa cells were cultured in DMEM supplemented with 10% FBS and 1% PenStrep. All the cells were maintained in a humidified incubator containing 5% CO₂ at 37 °C.

High-throughput Screening. The HTS was carried out at the HTS core facility of the University of Colorado at Boulder. Briefly, HEK hTLR7 cells were seeded in duplicate at 20,000 cells/well in a total volume of 50 µL/well in 384-well plates. Cells were stimulated with TLR7 agonist R848 (1µg/mL). The library compounds were dissolved in DMSO and used at 40 µM in the screening. Triptolide was used as a positive control at 40 nM. DMSO (0.4%) was the negative control. Various instruments such as CyBi-Well, 96- and 384-channel simultaneous pipettor, precision microplate pipetting system, EL406 combination washer dispenser, PlateLoc Thermal microplate sealer and EnVision multilabel plate reader were used to carry out the screening. The SEAP readouts were detected by QUANTI-Blue.

QUANTI-Blue SEAP assay. HEK hTLR cells were seeded at a density of 5×10^4 cells/well in 96-well plates for 24 h at 37 °C before treatment. The ligands for different TLRs are Pam3CSK4 (100 µg/mL) for hTLR1/2, Pam2CSK4 (100 µg/mL) for hTLR2/3, poly I:C (5 µg/mL) for hTLR3, LPS (20 ng/mL) for hTLR4, flagellin (100 ng/mL) for hTLR5, R848 (1 µg/mL) for hTLR7 and hTLR8, and CpG-ODN2006 (1 µg/mL) for hTLR9. After treatment for 24 h, a sample buffer (20 µL) from each well of the cell culture supernatants was collected and transferred to a transparent 96-well plate. Each well was treated with 180 µL of QUANTI-Blue buffer and incubated at 37 °C for 1 h. Optical density was measured using a plate reader (Beckman Coulter, DTX 880) at an absorbance of 620 nm.

WST-1 Assay for Cell Viability. HEK hTLR cells were seeded at a density of 5×10^4 cells/well in 100 μ L of culture medium in 96-well plates and incubated for 24 h. A series of concentrations of indicated compounds were added to the wells and incubated for additional 24 h. WST-1 proliferation reagent (10 μ L/well) was added and incubated at 37 °C until a color change was observed (30 min to 2 h). Data were quantified on a Beckman-Coulter DTX 880 Multimode Detector using absorbance at 450 nm.

Western Blot Analysis. RAW 264.7 cells were seeded in 10-cm cell-culture dishes at a density of 3×10^6 cells per dish and cultured overnight. Cells were then treated with **Z9j** for 1 h prior to LPS (100 ng/mL) stimulation in a humidified incubator at 37 °C for indicated time. The cells were rinsed with ice-cold PBS and lysed in nuclear and cytoplasmic protein extraction reagents with protease and phosphatase inhibitor cocktails. The protein concentration of each sample was determined using a Pierce BCA protein assay kit. Appropriate amount of total protein (20-30 μ g) were denatured, subjected to SDS-PAGE using a 10% running gel, transferred to nitrocellulose membrane. The nitrocellulose membrane was blocked with 5% BSA at room temperature for 1 h and incubated with indicated antibodies at 4 °C overnight, and then incubated with an anti-rabbit IgG, HRP-linked secondary antibody for 1 h. The signals were detected by ECL. The results were evaluated by densitometry analysis.

Src Kinase Assay. The activity of Src was determined by using Src kinase, Src substrate (KVEKIGEGTYGVVYK-amide) and an ADP-Glo kinase assay kit per manufacturer's specifications. The ATP concentration used in the kinase assay was 100 μ M.

TNF- α ELISA. RAW 264.7 cells were seeded at a density of 1.5×10^6 cells/well in six-well plates and grown at 37°C in a 5% CO₂ humidified incubator. After 24 h, nonadherent cells and medium were removed and replaced with fresh DMEM medium (3 mL per well). The cells were

1
2
3 treated with LPS (100 ng/ml) in the presence or absence of different concentrations of **Z9j** for 18
4
5 h. The cell culture supernatants were collected and frozen at -80°C until ready for cytokine
6
7 measurement. The production of the cytokine TNF- α was quantified using cytokine-specific
8
9 capture antibodies, detection antibodies, and recombinant mouse cytokine standards according to
10
11 a commercially available ELISA kit per manufacturer's specifications.
12
13

14
15 **DAN Assay.** RAW 264.7 cells were plated at a density of 2×10^5 cells/mL in 96-well culture
16
17 plate at 37°C in a 5% CO₂ humidified incubator. After 24 h, nonadherent cells and medium were
18
19 removed and replaced with fresh DMEM medium. The adherent macrophages were treated with
20
21 and LPS (100 ng/ml) in the presence or absence of different concentrations of **Z9j** for 18 h. The
22
23 nitrite concentration in the culture medium was measured as an indicator of NO production.
24
25 Briefly, 100 μ L of medium was collected and added to flat black 96-well microfluor plates. To
26
27 each well, 10 μ L of 2,3-diaminonaphthalene (0.05 mg/ml in 0.62 M aqueous HCl solution) was
28
29 added and incubated for 15 min in the dark. The reaction was quenched by addition of 5 μ L of a
30
31 3 M aqueous NaOH solution, and the plate was read on a Beckman Coulter DTX 880 reader with
32
33 excitation at 365 nm and emission at 450 nm. NO production by LPS stimulation was designated
34
35 as 100% for each experiment.
36
37
38
39

40
41 **WST-1 Assay for Cell Growth Inhibition.** HeLa cells or HuMECs were seeded at a density
42
43 of 5×10^3 cells/well in 100 μ L of culture medium in 96-well plates and incubated for 24 h. A
44
45 series of concentrations of indicated compounds were added to the wells and incubated for
46
47 additional 24 or 48 h. WST-1 proliferation reagent (10 μ L/well) was added and incubated at 37
48
49 °C until a color change was observed (30 min to 2 h). Data were quantified on a Beckman-
50
51 Coulter DTX 880 Multimode Detector using absorbance at 450 nm. Growth inhibition (%) was
52
53
54
55
56
57
58
59
60

determined using the following formula: Growth inhibition (%) = $(1 - [\text{Compounds (OD}_{450}) - \text{Background (OD}_{450})] / [\text{Control (OD}_{450}) - \text{Background (OD}_{450})]) \times 100$.

Apoptosis Assay. HeLa cells were seeded at a density of 3×10^5 cells/well in six-well plates and allowed to attach for 24 h. After treatment of indicated concentrations of **Z9j** or DMSO control for another 24 h, cells were harvested with 0.25% trypsin without ethylenediaminetetraacetic acid (EDTA) and rinsed twice with PBS, then stained using an Annexin V-FITC apoptosis detection kit per manufacturer's instructions. Cells were analyzed with a BD Accuri C6 flow cytometer.

Cell Cycle Analysis. HeLa cells were seeded at a density of 3×10^5 cells/well in six-well plates and allowed to attach overnight. The culture medium was changed to serum-free to facilitate cycle synchronization prior to treatment with indicated concentrations of **Z9j** or DMSO control. After 24 h, cells were harvested with 0.25% trypsin without EDTA, washed twice with assay buffer and pelleted. Cell pellets were fixed and stained using a Cell Cycle Phase Determination kit per manufacturer's specifications. Cells were analyzed with a BD Accuri C6 flow cytometer.

Statistical Analysis. All data from cell culture experiments were performed on the basis of three individual cell preparations unless otherwise noted. Data are expressed as mean \pm SD. Statistical significances were determined with use of the unpaired Student's *t* test. Values of *p* < 0.05 were considered as statistically significant.

ASSOCIATED CONTENT

Supporting Information. The Supporting Information is available free of charge on the ACS Publications website at DOI: xxxxxxxxx.

Figure S1. Dose-response curve of triptolide by the SEAP assay in HEK hTLR7 cells. ^1H and ^{13}C NMR spectra for all the products (PDF)

Molecular formula strings (CSV)

AUTHOR INFORMATION

Corresponding Author

*E-mail: hubert.yin@colorado.edu. Tel: +1 303 492 6786.

ORCID

Lei Zhang: 0000-0001-7409-6090.

Lei Shi: 0000-0002-3820-3693.

Shafer Myers Soars: 0000-0003-3516-9335.

Joshua Kamps: 0000-0002-3539-0227.

Hang Yin: 0000-0002-9762-4818.

Notes

The authors declare no competing financial interest.

Author Contributions.

L.Z. executed the project including performing and analyzing the HTS, chemical synthesis, SAR studies, and all biological tests. L.S. participated in the chemical synthesis, SAR studies, SEAP, WST-1, and nitric oxide assays. S.M.S. participated in the SEAP and nitric oxide assays. J.K. performed the HPLC analysis. L.Z., L.S., and H.Y. wrote the manuscript. All authors read and approved the final manuscript.

ACKNOWLEDGMENTS

We are grateful to Prof. Xiang Wang and Dr. Wei Wang for assistance with the high-throughput screening. We thank Dr. Christina Boville for helpful discussions.

Funding Sources. This study was supported by grants from National Institutes of Health (R35GM127003) and China Scholarship Council (201407060053 for L.S.).

ABBREVIATIONS USED

NF- κ B, nuclear factor- κ B; NEMO, NF- κ B essential modulator; TLR, Toll-like receptor; TNFR, tumor necrosis factor receptor; IL-1R, interleukin-1 receptor; TCR, T cell receptor; BCR, B cell receptor; PAMPs, pathogen-associated molecular patterns; DAMPs, danger-associated molecular patterns; LPS, lipopolysaccharide; NO, nitric oxide; HTS, high-throughput screening; SAR, structure-activity relationship; HEK293, human embryonic kidney 293; SEAP, secreted embryonic alkaline phosphatase; RMS, root mean square; IC₅₀, half-maximal inhibitory concentration; PKC, protein kinase C; PMA, phorbol 12-myristate 13-acetate; iNOS, inducible nitric oxide synthase; DAN, 2,3-diaminonaphthalene; IFN- γ , interferon γ ; PI3K, phosphatidylinositol-3-kinase; MAPK, mitogen-activated protein kinase; JNK, c-Jun N-terminal kinase; ERK, extracellular signal regulated protein kinase; AP-1, activator protein 1; Syk, spleen tyrosine kinase; ELISA, enzyme-linked immunosorbent assay; GI₅₀, growth inhibition of 50%; HuMEC, human mammary epithelial cell; PI, propidium iodide; ECL, enhanced chemiluminescence; DMEM, Dulbecco's modified Eagle's medium; FBS, fetal bovine serum; EDTA, ethylenediaminetetraacetic acid.

REFERENCES

- (1) Zhang, Q.; Lenardo, M. J.; Baltimore, D. 30 years of NF- κ B: a blossoming of relevance to human pathobiology. *Cell* **2017**, *168*, 37-57.
- (2) Israel, A. The IKK complex, a central regulator of NF- κ B activation. *Cold Spring Harb. Perspect. Biol.* **2010**, *2*, a000158.

- (3) Hayden, M. S.; Ghosh, S. Shared principles in NF- κ B signaling. *Cell* **2008**, *132*, 344-362.
- (4) O'Dea, E.; Hoffmann, A. The regulatory logic of the NF- κ B signaling system. *Cold Spring Harb. Perspect. Biol.* **2010**, *2*, a000216.
- (5) Pahl, H. L. Activators and target genes of Rel/NF- κ B transcription factors. *Oncogene* **1999**, *18*, 6853-6866.
- (6) Basak, S.; Hoffmann, A. Crosstalk via the NF- κ B signaling system. *Cytokine Growth Factor Rev.* **2008**, *19*, 187-197.
- (7) Hayden, M. S.; Ghosh, S. Signaling to NF- κ B. *Gene Dev.* **2004**, *18*, 2195-2224.
- (8) Verstrepen, L.; Bekaert, T.; Chau, T. L.; Tavernier, J.; Chariot, A.; Beyaert, R. TLR-4, IL-1R and TNF-R signaling to NF- κ B: variations on a common theme. *Cell. Mol. Life Sci.* **2008**, *65*, 2964-2978.
- (9) Carmody, R. J.; Chen, Y. H. Nuclear factor- κ B: activation and regulation during Toll-like receptor signaling. *Cell. Mol. Immunol.* **2007**, *4*, 31-41.
- (10) Kawai, T.; Akira, S. Signaling to NF- κ B by Toll-like receptors. *Trends Mol. Med.* **2007**, *13*, 460-469.
- (11) Baker, R. G.; Hayden, M. S.; Ghosh, S. NF- κ B, inflammation, and metabolic disease. *Cell Metab.* **2011**, *13*, 11-22.
- (12) Chung, H. Y.; Cesari, M.; Anton, S.; Marzetti, E.; Giovannini, S.; Seo, A. Y.; Carter, C.; Yu, B. P.; Leeuwenburgh, C. Molecular inflammation: underpinnings of aging and age-related diseases. *Ageing Res. Rev.* **2009**, *8*, 18-30.
- (13) Tilstra, J. S.; Clauson, C. L.; Niedernhofer, L. J.; Robbins, P. D. NF- κ B in aging and disease. *Aging Dis.* **2011**, *2*, 449-465.

- (14) Sun, Z.; Andersson, R. NF- κ B activation and inhibition: a review. *Shock* **2002**, *18*, 99-106.
- (15) Liu, T.; Zhang, L.; Joo, D.; Sun, S. C. NF- κ B signaling in inflammation. *Signal Transduct. Target. Ther.* **2017**, *2*, e17023.
- (16) Dinarello, C. A. Anti-inflammatory agents: present and future. *Cell* **2010**, *140*, 935-950.
- (17) Tabas, I.; Glass, C. K. Anti-inflammatory therapy in chronic disease: challenges and opportunities. *Science* **2013**, *339*, 166-172.
- (18) Amiri, K. I.; Richmond, A. Role of nuclear factor- κ B in melanoma. *Cancer Metast. Rev.* **2005**, *24*, 301-313.
- (19) Bours, V.; Bentires-Alj, M.; Hellin, A. C.; Viatour, P.; Robe, P.; Delhalle, S.; Benoit, V.; Merville, M. P. Nuclear factor- κ B, cancer, and apoptosis. *Biochem. Pharmacol.* **2000**, *60*, 1085-1089.
- (20) Xia, Y.; Shen, S.; Verma, I. M. NF- κ B, an active player in human cancers. *Cancer Immunol Res.* **2014**, *2*, 823-830.
- (21) Erstad, D. J.; Cusack, J. C., Jr. Targeting the NF- κ B pathway in cancer therapy. *Surg. Oncol. Clin. N. Am.* **2013**, *22*, 705-746.
- (22) Li, F.; Zhang, J.; Arfuso, F.; Chinnathambi, A.; Zayed, M. E.; Alharbi, S. A.; Kumar, A. P.; Ahn, K. S.; Sethi, G. NF- κ B in cancer therapy. *Arch. Toxicol.* **2015**, *89*, 711-731.
- (23) Gupta, S. C.; Sundaram, C.; Reuter, S.; Aggarwal, B. B. Inhibiting NF- κ B activation by small molecules as a therapeutic strategy. *BBA Gene Regul. Mech.* **2010**, *1799*, 775-787.
- (24) Gilmore, T. D.; Herscovitch, M. Inhibitors of NF- κ B signaling: 785 and counting. *Oncogene* **2006**, *25*, 6887-6899.

(25) Herrington, F. D.; Carmody, R. J.; Goodyear, C. S. Modulation of NF- κ B signaling as a therapeutic target in autoimmunity. *J. Biomol. Screen.* **2016**, *21*, 223-242.

(26) Panday, A.; Inda, M. E.; Bagam, P.; Sahoo, M. K.; Osorio, D.; Batra, S. Transcription factor NF- κ B: an update on intervention strategies. *Arch. Immunol. Ther. Exp.* **2016**, *64*, 463-483.

(27) Ruland, J. Return to homeostasis: downregulation of NF- κ B responses. *Nat. Immunol.* **2011**, *12*, 709-714.

(28) Hertzberg, R. P.; Pope, A. J. High-throughput screening: new technology for the 21st century. *Curr. Opin. Chem. Biol.* **2000**, *4*, 445-451.

(29) An, W. F.; Tolliday, N. Cell-based assays for high-throughput screening. *Mol. Biotechnol.* **2010**, *45*, 180-186.

(30) Zhang, L.; Dewan, V.; Yin, H. Discovery of small molecules as multi-Toll-like receptor agonists with proinflammatory and anticancer activities. *J. Med. Chem.* **2017**, *60*, 5029-5044.

(31) Salyer, A. C. D.; Caruso, G.; Khetani, K. K.; Fox, L. M.; Malladi, S. S.; David, S. A. Identification of adjuvant activity of amphotericin B in a novel, multiplexed, poly-TLR/NLR high-throughput screen. *PLOS ONE* **2016**, *11*, e0149848.

(32) Zhang, J. H.; Chung, T. D. Y.; Oldenburg, K. R. A simple statistical parameter for use in evaluation and validation of high throughput screening assays. *J. Biomol. Screen.* **1999**, *4*, 67-73.

(33) Qiu, D.; Zhao, G.; Aoki, Y.; Shi, L.; Uyei, A.; Nazarian, S.; Ng, J. C.; Kao, P. N. Immunosuppressant PG490 (triptolide) inhibits T-cell interleukin-2 expression at the level of purine-box/nuclear factor of activated T-cells and NF- κ B transcriptional activation. *J. Biol. Chem.* **1999**, *274*, 13443-13450.

(34) Ziaei, S.; Halaby, R. Immunosuppressive, anti-inflammatory and anti-cancer properties of triptolide: a mini review. *Avicenna J. Phytomed.* **2016**, *6*, 149-164.

(35) Nishizuka, Y. Protein kinase C and lipid signaling for sustained cellular responses. *FASEB J.* **1995**, *9*, 484-496.

(36) Lee, J.; Mira-Arbibe, L.; Ulevitch, R. J. TAK1 regulates multiple protein kinase cascades activated by bacterial lipopolysaccharide. *J. Leukocyte. Biol.* **2000**, *68*, 909-915.

(37) Hattori, Y.; Hattori, S.; Kasai, K. Lipopolysaccharide activates Akt in vascular smooth muscle cells resulting in induction of inducible nitric oxide synthase through nuclear factor- κ B activation. *Eur. J. Pharmacol.* **2003**, *481*, 153-158.

(38) Pahan, K.; Raymond, J. R.; Singh, I. Inhibition of phosphatidylinositol 3-kinase induces nitric-oxide synthase in lipopolysaccharide- or cytokine-stimulated C6 glial cells. *J. Biol. Chem.* **1999**, *274*, 7528-7536.

(39) Park, Y. C.; Lee, C. H.; Kang, H. S.; Chung, H. T.; Kim, H. D. Wortmannin, a specific inhibitor of phosphatidylinositol-3-kinase, enhances LPS-induced NO production from murine peritoneal macrophages. *Biochem. Bioph. Res. Comm.* **1997**, *240*, 692-696.

(40) Kyriakis, J. M.; Avruch, J. Mammalian MAPK signal transduction pathways activated by stress and inflammation: a 10-year update. *Physiol. Rev.* **2012**, *92*, 689-737.

(41) Plotnikov, A.; Zehorai, E.; Procaccia, S.; Seger, R. The MAPK cascades: signaling components, nuclear roles and mechanisms of nuclear translocation. *BBA Mol. Cell Res.* **2011**, *1813*, 1619-1633.

(42) Zhang, Y.; Dong, C. Regulatory mechanisms of mitogen-activated kinase signaling. *Cell Mol. Life Sci.* **2007**, *64*, 2771-2789.

(43) Beitz, L. O.; Fruman, D. A.; Kurosaki, T.; Cantley, L. C.; Scharenberg, A. M. Syk is upstream of phosphoinositide 3-kinase in B cell receptor signaling. *J. Biol. Chem.* **1999**, *274*, 32662-32666.

(44) Pleiman, C.; Hertz, W.; Cambier, J. Activation of phosphatidylinositol-3' kinase by Src-family kinase SH3 binding to the p85 subunit. *Science* **1994**, *263*, 1609-1612.

(45) Hoesel, B.; Schmid, J. A. The complexity of NF- κ B signaling in inflammation and cancer. *Mol. Cancer* **2013**, *12*, 86.

(46) Oeckinghaus, A.; Hayden, M. S.; Ghosh, S. Crosstalk in NF- κ B signaling pathways. *Nat. Immunol.* **2011**, *12*, 695-708.

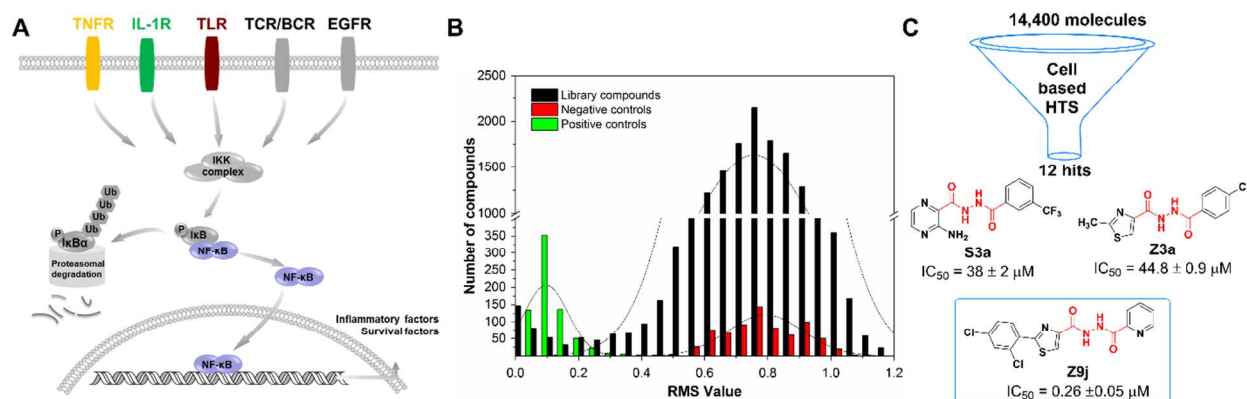
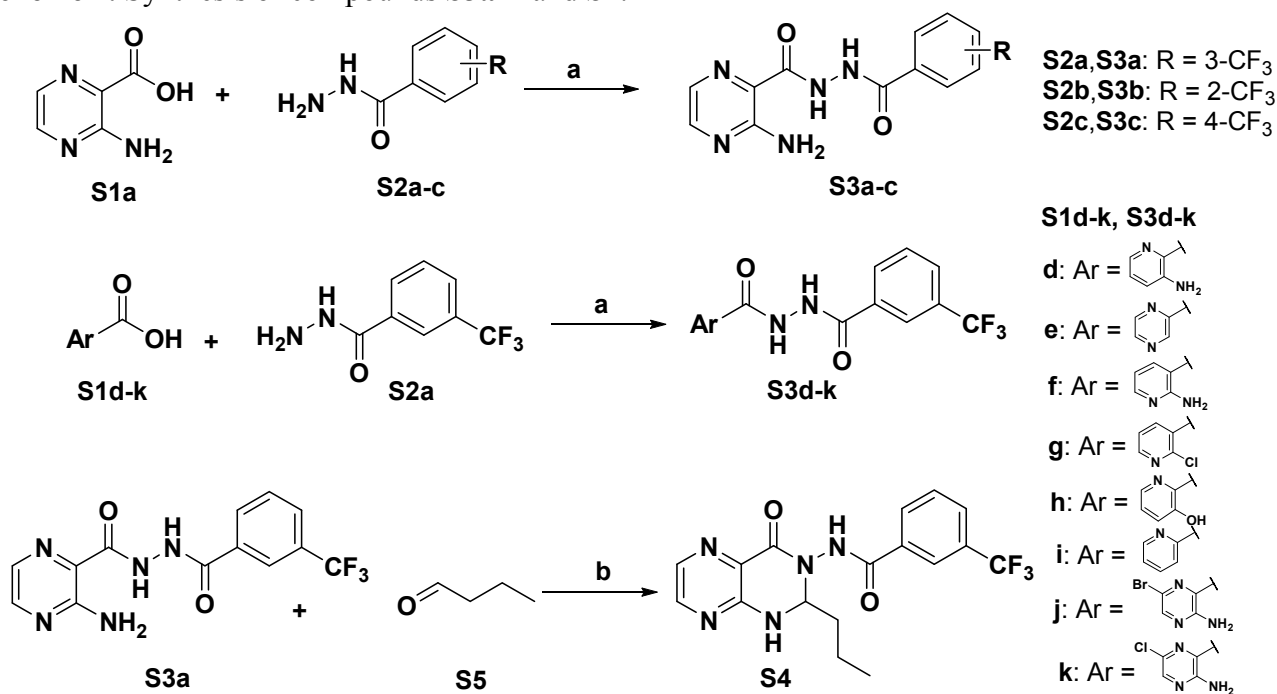
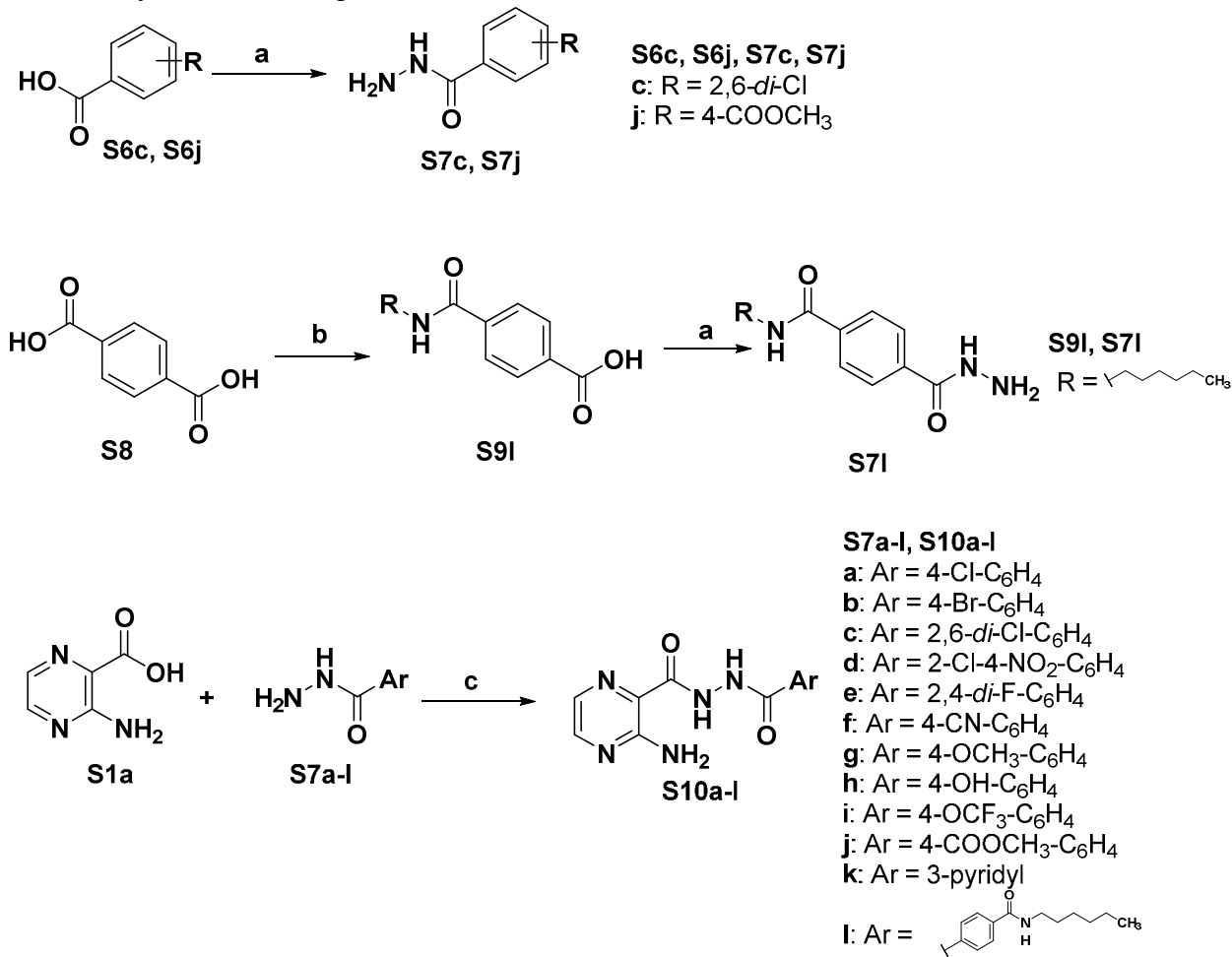


Figure 1. (A) Multiple signaling pathways converge on NF- κ B activation. (B) Histogram depicting the data distribution from the HTS. A total of 14,400 compounds from the Maybridge HitFinder v11 library along with the positive and the negative controls were distributed based on the RMS values. $RMS = \sqrt{\frac{a_1^2 + a_2^2}{2}}$, where a_1 and a_2 represent the duplicate set of values for positive, negative, and test controls after subtraction of background values in each plate. (C) Structures and activities of compounds **S3a**, **Z3a**, and **Z9j**.

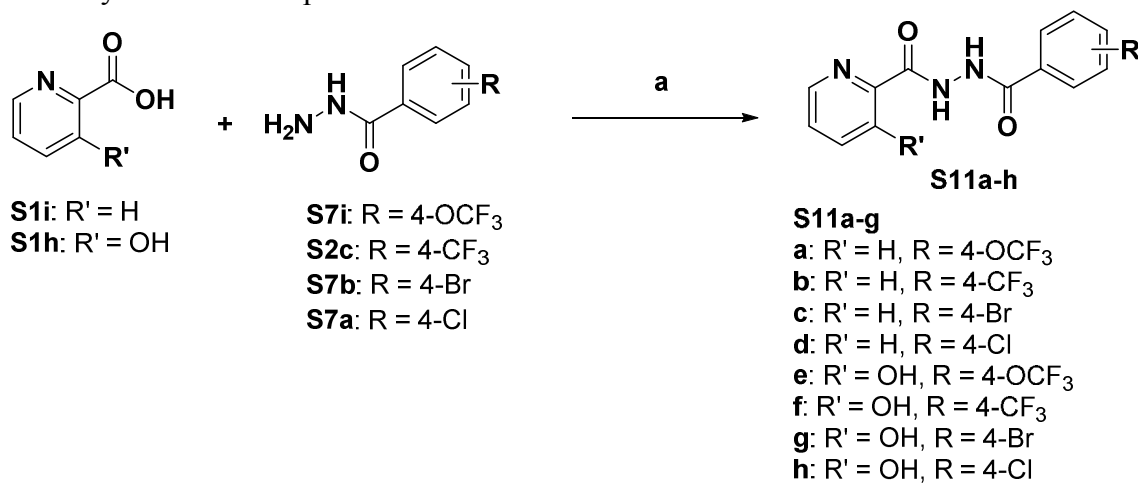
Scheme 1. Synthesis of compounds **S3a-k** and **S4**.^a

^aReagents and conditions: (a) TBTU, Et₃N, DMF, rt; (b) *p*-toluenesulfonic acid monohydrate, dioxane, reflux, 2 h.

Scheme 2. Synthesis of compounds **S10a-l**.^a

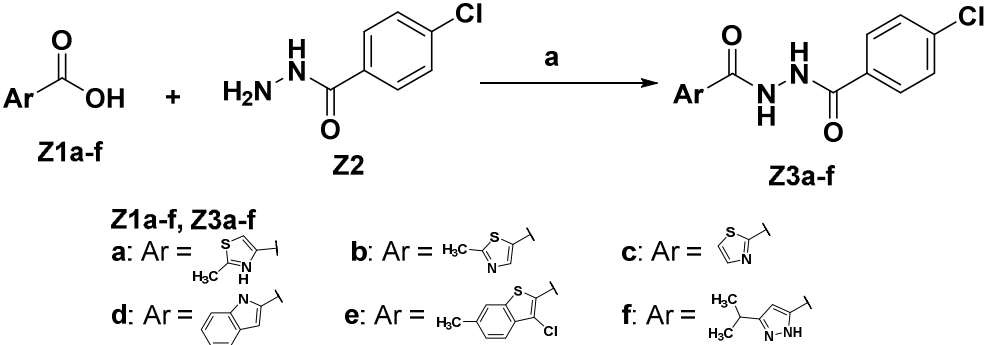


^aReagents and conditions: (a) hydrazine, HOBt, EDCI, DMF, rt; (b) HOBt, EDCI, DIPEA, DMF, rt; (c) TBTU, Et₃N, DMF, rt.

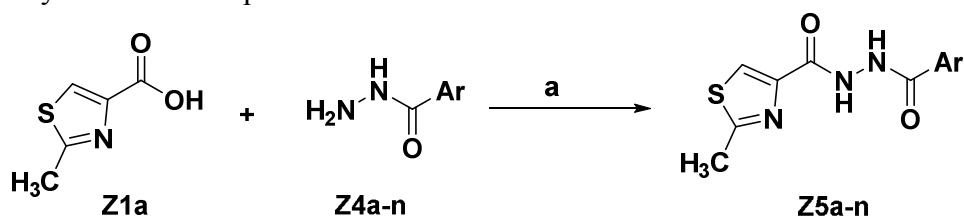
Scheme 3. Synthesis of compounds S11a-h.^a

^aReagents and conditions: (a) TBTU, Et₃N, DMF, rt.

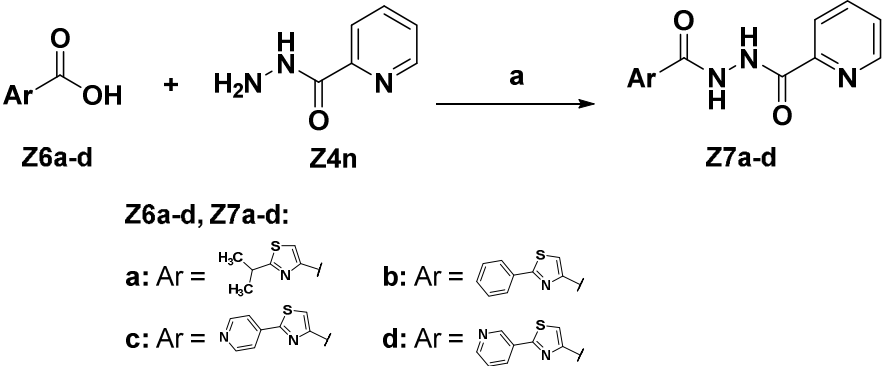
Scheme 4. Synthesis of compounds **Z3a-f**.^a



^aReagents and conditions: (a) TBTU, Et₃N, DMF, rt.

Scheme 5. Synthesis of compounds **Z5a-n**.^a**Z4a-n, Z5a-n****a**: Ar = 2-Cl-C₆H₄**b**: Ar = 3-Cl-C₆H₄**c**: Ar = 3-CN-C₆H₄**d**: Ar = 3-COOCH₃-C₆H₄**e**: Ar = 3-F-C₆H₄**f**: Ar = 3-Br-C₆H₄**g**: Ar = 3-OH-C₆H₄**h**: Ar = 3-CF₃-C₆H₄**i**: Ar = 3,5-di-Cl-C₆H₄**j**: Ar = 3-OCF₃-C₆H₄**k**: Ar = 3-OCH₃-C₆H₄**l**: Ar = 2-pyridyl**m**: Ar = 3-pyridyl**n**: Ar = 4-pyridyl^aReagents and conditions: (a) TBTU, Et₃N, DMF, rt.

Scheme 6. Synthesis of compounds **Z7a-d**.^a



^aReagents and conditions: (a) TBTU, Et₃N, DMF, rt.

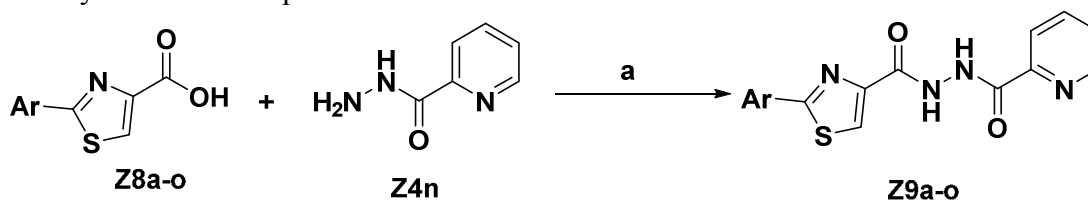
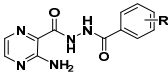
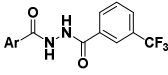
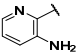
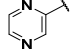
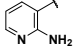
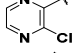
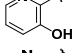
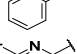
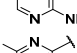
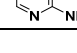
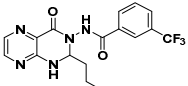
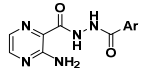
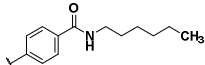
Scheme 7. Synthesis of compounds **Z9a-o**.^a**Z9a-o, Z10a-o****a:** Ar = 4-F-C₆H₄**b:** Ar = 4-Cl-C₆H₄**c:** Ar = 4-CF₃-C₆H₄**d:** Ar = 4-CH₃-C₆H₄**e:** Ar = 4-CH₂CH₃-C₆H₄**f:** Ar = 4-OCH₃-C₆H₄**g:** Ar = 4-N(CH₃)₂-C₆H₄**h:** Ar = 3,4-di-OCH₃-C₆H₄**i:** Ar = 2,3-di-Cl-C₆H₄**j:** Ar = 2,4-di-Cl-C₆H₄**k:** Ar = 3,5-di-Cl-C₆H₄**l:** Ar = 3-F-C₆H₄**m:** Ar = 3-Cl-C₆H₄**n:** Ar = 3-Br-C₆H₄**o:** Ar = 3-CF₃-C₆H₄^aReagents and conditions: (a) TBTU, Et₃N, DMF, rt.

Table 1. SAR studies of compounds **S3a-k** and **S4** in HEK hTLR7 cells.

Structure		Compd	TLR7-mediated NF-κB activation	
Generic structure	R/Ar		% Inhibition (40 μM) ^a	IC ₅₀ (μM) ^a
	3-CF ₃	S3a	68 ± 2	38 ± 2
	2-CF ₃	S3b	23 ± 4	n.d. ^b
	4-CF ₃	S3c	79 ± 3	25 ± 6
		S3d	83.1 ± 0.8	16 ± 3
		S3e	29 ± 1	n.d.
		S3f	22 ± 2	n.d.
		S3g	19 ± 3	n.d.
		S3h	96 ± 1	14.2 ± 0.7
		S3i	88 ± 1	15 ± 1
		S3j	18.2 ± 0.4	n.d.
		S3k	21 ± 2	n.d.
		S4	21 ± 3	n.d.

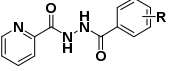
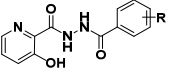
^an = 2 (mean ± SD). ^bn.d.: not determined.

Table 2. SAR studies of compounds **S10a-l** in HEK hTLR7 cells.

Structure		Compd	TLR7-mediated NF-κB activation	
Generic structure	Ar		% Inhibition (40 μM) ^a	IC ₅₀ (μM) ^a
	4-Cl-C ₆ H ₄	S10a	42 ± 3	n.d.
	4-Br-C ₆ H ₄	S10b	36.2 ± 0.7	n.d.
	2,6- <i>di</i> -Cl-C ₆ H ₄	S10c	28 ± 1	n.d.
	2-Cl-4-NO ₂ -C ₆ H ₄	S10d	23 ± 2	n.d.
	2,4- <i>di</i> -F-C ₆ H ₄	S10e	26 ± 3	n.d.
	4-CN-C ₆ H ₄	S10f	15 ± 5	n.d.
	4-OCH ₃ -C ₆ H ₄	S10g	20.4 ± 0.7	n.d.
	4-OH-C ₆ H ₄	S10h	17.7 ± 0.6	n.d.
	4-OCF ₃ -C ₆ H ₄	S10i	72 ± 1	27 ± 2
	4-COOCH ₃ -C ₆ H ₄	S10j	18 ± 1	n.d.
	3-pyridyl	S10k	12.0 ± 0.5	n.d.
		S10l	17 ± 2	n.d.

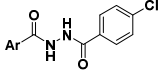
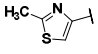
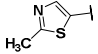
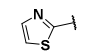
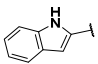
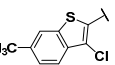
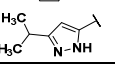
^an = 2 (mean ± SD). ^bn.d.: not determined.

Table 3. SAR studies of compounds **S11a-h** in HEK hTLR7 cells.

Structure		Compd	TLR7-mediated NF-κB activation	
Generic structure	R		% Inhibition (40 μM) ^a	IC ₅₀ (μM) ^a
	4-OCF ₃	S11a	79.8 ± 0.8	22 ± 1
	4-CF ₃	S11b	85.4 ± 0.6	17 ± 1
	4-Br	S11c	82.3 ± 0.6	17 ± 2
	4-Cl	S11d	76 ± 2	24.7 ± 0.8
	4-OCF ₃	S11e	96.5 ± 0.2	7.9 ± 0.5
	4-CF ₃	S11f	97.4 ± 0.2	13.4 ± 0.3
	4-Br	S11g	96.18 ± 0.07	17.26 ± 0.09
	4-Cl	S11h	81 ± 4	27.8 ± 0.5

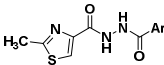
^an = 2 (mean ± SD).

Table 4. SAR studies of compounds **Z3a-f** in HEK hTLR7 cells.

Structure		Compd	TLR7-mediated NF-κB activation	
Generic structure	Ar		% Inhibition (40 μM) ^a	IC ₅₀ (μM) ^a
		Z3a	51 ± 2	44.8 ± 0.9
		Z3b	17.0 ± 0.4	n.d. ^b
		Z3c	24 ± 1	n.d.
		Z3d	13 ± 2	n.d.
		Z3e	16.7 ± 0.5	n.d.
		Z3f	11 ± 2	n.d.

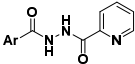
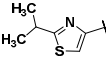
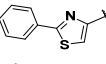
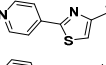
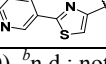
^an = 2 (mean ± SD). ^bn.d.: not determined.

Table 5. SAR studies of compounds **Z5a-n** in HEK hTLR7 cells.

Structure		Compd	TLR7-mediated NF-κB activation	
Generic structure	Ar		% Inhibition (40 μM) ^a	IC ₅₀ (μM) ^a
	4-Cl-C ₆ H ₄	Z3a	51 ± 2	44.8 ± 0.9
	2-Cl-C ₆ H ₄	Z5a	6 ± 1	n.d. ^b
	3-Cl-C ₆ H ₄	Z5b	40 ± 6	60 ± 3
	3-CN-C ₆ H ₄	Z5c	6.4 ± 0.8	n.d.
	3-COOCH ₃ -C ₆ H ₄	Z5d	9 ± 4	n.d.
	3-F-C ₆ H ₄	Z5e	21.1 ± 0.2	n.d.
	3-Br-C ₆ H ₄	Z5f	30.6 ± 0.8	n.d.
	3-OH-C ₆ H ₄	Z5g	18 ± 4	n.d.
	3-CF ₃ -C ₆ H ₄	Z5h	31 ± 2	n.d.
	3,5-di-Cl-C ₆ H ₄	Z5i	24 ± 7	n.d.
	3-OCF ₃ -C ₆ H ₄	Z5j	26 ± 3	n.d.
	3-OCH ₃ -C ₆ H ₄	Z5k	24 ± 1	n.d.
	2-pyridyl	Z5l	73 ± 2	30 ± 2
	3-pyridyl	Z5m	21.0 ± 0.4	n.d.
	4-pyridyl	Z5n	19.5 ± 1.6	n.d.

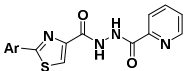
^an = 2 (mean ± SD). ^bn.d.: not determined.

Table 6. SAR studies of compounds **Z7a-d** in HEK hTLR7 cells.

Structure		Comp	TLR7-mediated NF-κB activation	
Generic structure	Ar		% Inhibition (40 μM) ^a	IC ₅₀ (μM) ^a
		Z7a	94.2 ± 0.9	14 ± 1
		Z7b	98.8 ± 0.2	5.8 ± 0.3
		Z7c	33 ± 3	n.d. ^b
		Z7d	86 ± 1	23.2 ± 0.8

^an = 2 (mean ± SD). ^bn.d.: not determined.

Table 7. SAR studies of compounds **Z9a-o** in HEK hTLR7 cells.

Structure		Compd	TLR7-mediated NF-κB activation	
Generic structure	Ar		% Inhibition (5 μM) ^a	IC ₅₀ (μM) ^a
	4-F-C ₆ H ₄	Z9a	65 ± 3	4.4 ± 0.3
	4-Cl-C ₆ H ₄	Z9b	91 ± 1	2.1 ± 0.2
	4-CF ₃ -C ₆ H ₄	Z9c	96.1 ± 0.4	0.99 ± 0.09
	4-CH ₃ -C ₆ H ₄	Z9d	88.2 ± 0.5	1.83 ± 0.08
	4-CH ₂ CH ₃ -C ₆ H ₄	Z9e	91.9 ± 0.4	2.4 ± 0.2
	4-OCH ₃ -C ₆ H ₄	Z9f	80.3 ± 0.8	3.09 ± 0.07
	4-N(CH ₃) ₂ -C ₆ H ₄	Z9g	93.1 ± 0.3	1.9 ± 0.1
	3,4- <i>di</i> -OCH ₃ -C ₆ H ₄	Z9h	66 ± 1	3.9 ± 0.1
	2,3- <i>di</i> -Cl-C ₆ H ₄	Z9i	99.9 ± 0.1	0.50 ± 0.04
	2,4- <i>di</i> -Cl-C ₆ H ₄	Z9j (CU-CPT-Z9j)	99.6 ± 0.2	0.26 ± 0.05
	3,5- <i>di</i> -Cl-C ₆ H ₄		99.1 ± 0.2	0.44 ± 0.03
	3-F-C ₆ H ₄		79 ± 2	2.6 ± 0.2
	3-Cl-C ₆ H ₄	Z9m	93.7 ± 0.5	1.0 ± 0.1
	3-Br-C ₆ H ₄	Z9n	97.6 ± 0.6	0.9 ± 0.1
	3-CF ₃ -C ₆ H ₄	Z9o	96.7 ± 0.2	1.02 ± 0.06

^an = 2 (mean ± SD).

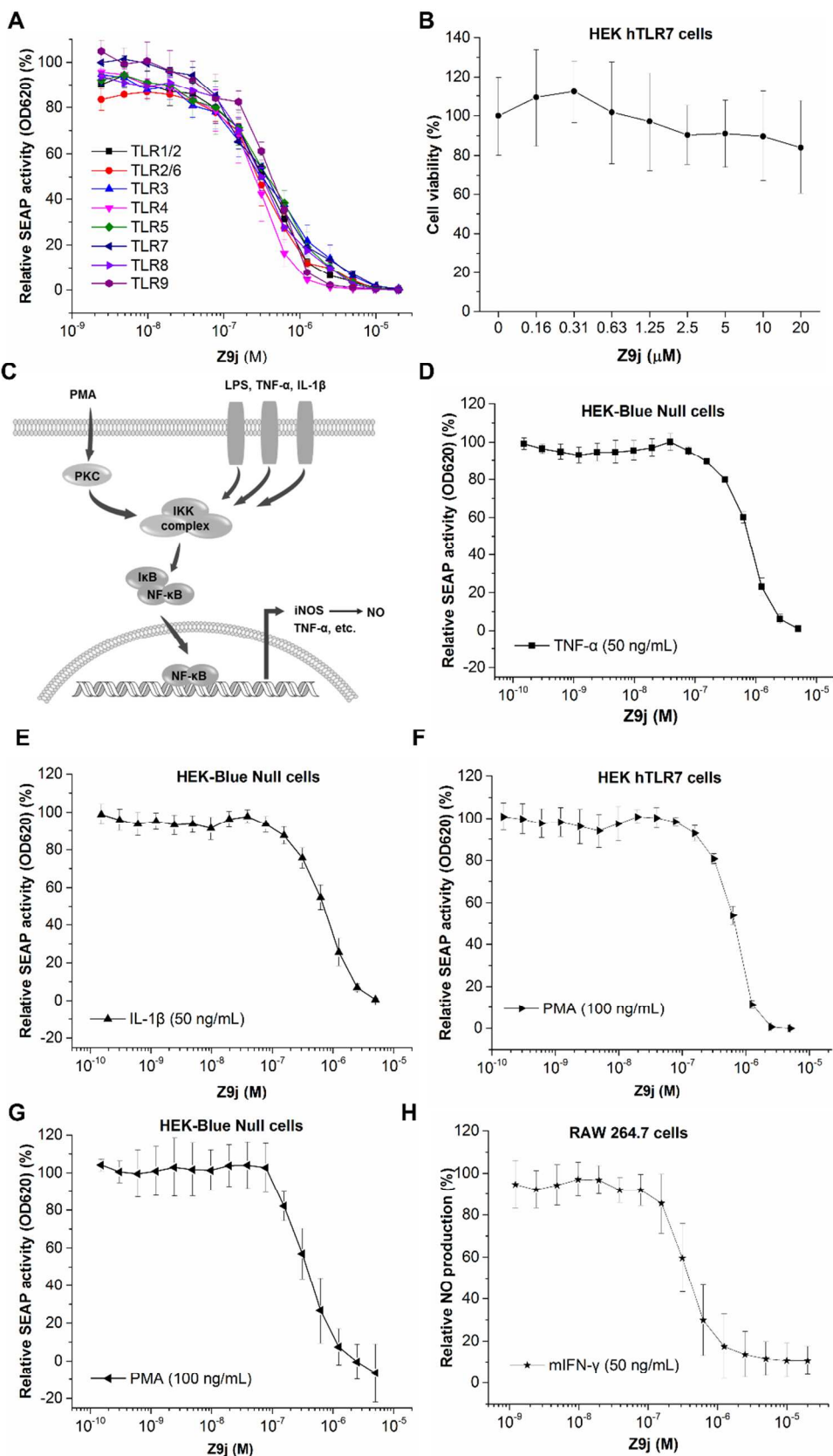


Figure 2. Mechanism of action study of Z9j by cellular approaches. (A) **Z9j** inhibited NF- κ B activation mediated by different TLRs in a similar manner. HEK293 cells were transfected with different human TLR genes and stimulated with different TLR ligands as follows: Pam3CSK4 (100 μ g/mL) for hTLR1/2, Pam2CSK4 (100 μ g/mL) for hTLR2/3, poly I:C (5 μ g/mL) for hTLR3, LPS (20 ng/mL) for hTLR4, flagellin (100 ng/mL) for hTLR5, R848 (1 μ g/mL) for hTLR7 and hTLR8, and CpG-ODN2006 (1 μ g/mL) for hTLR9. (B) Effect of **Z9j** on cell viability in HEK hTLR7 cells measured by the WST-1 assay. (C) Activation of TLRs, TNFR, IL-1R, and PKC all results in activation of NF- κ B signaling, leading to production of pro-inflammatory mediators such as TNF- α and NO. (D) **Z9j** inhibited TNF- α -induced NF- κ B activation in HEK-Blue Null cells. (E) **Z9j** inhibited IL-1 β -induced NF- κ B activation in HEK-Blue Null cells. (F) **Z9j** inhibited PMA-induced NF- κ B activation in HEK hTLR7 cells. (G) **Z9j** inhibited PMA-induced NF- κ B activation in HEK-Blue Null cells. (H) **Z9j** inhibited IFN- γ -induced NO production mediated by NF- κ B in mouse macrophage RAW 264.7 cells. n = 3 (mean \pm SD).

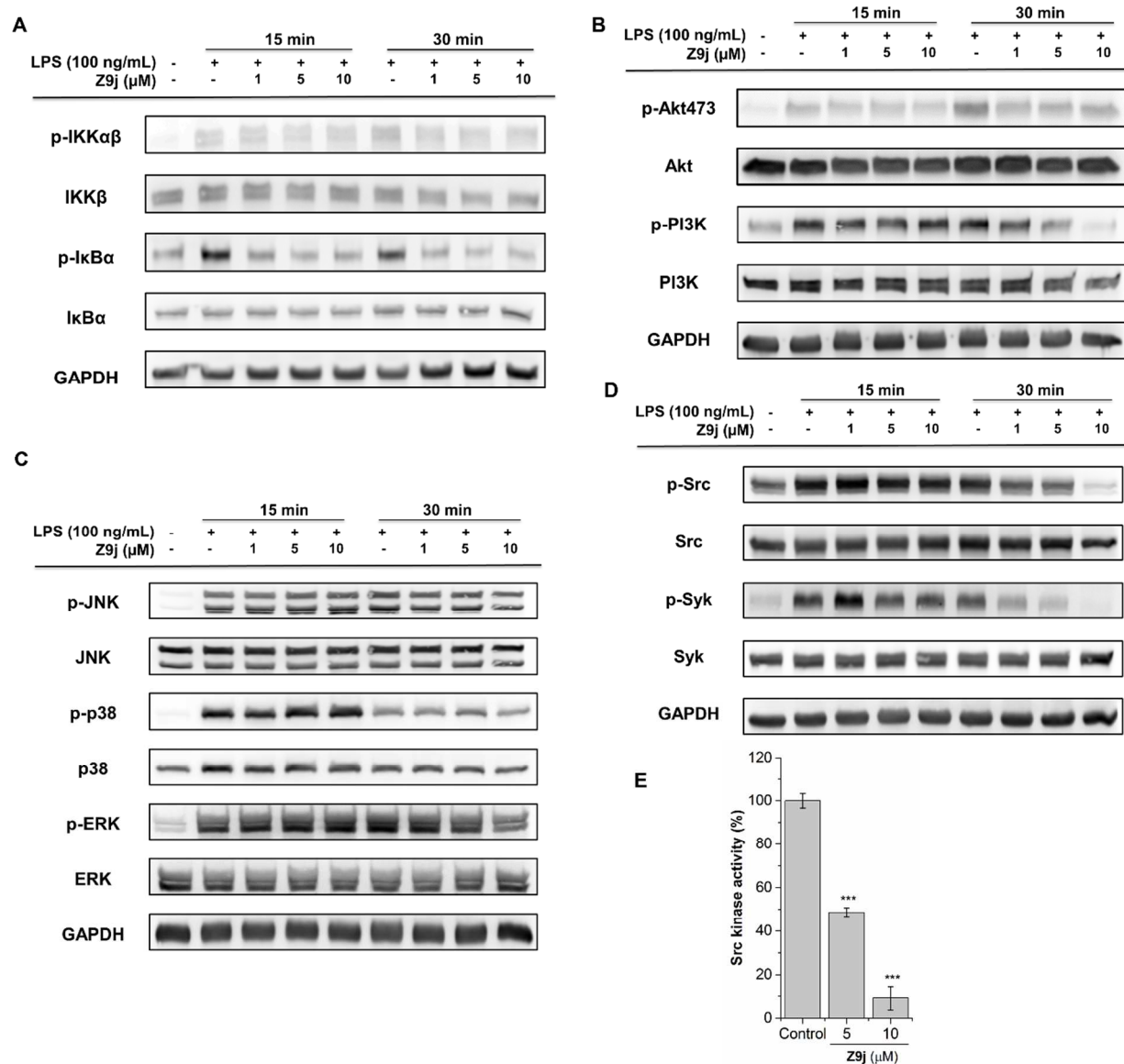


Figure 3. Mechanism of action study of Z9j by biochemical approaches. Macrophages RAW 264.7 cells were pre-treated with 1, 5, or 10 μ M of **Z9j** for 1 h, and then stimulated with LPS (100 ng/mL) for 15 min or 30 min as indicated. Phosph- and/or total (A) IKK $\alpha\beta$ and I κ B α , (B) JNK, p38, and ERK, (C) PI3K and Akt, and (D) Src and Syk were detected by Western blotting. GAPDH was used as a control. Each immunoblotting trace shown in the figures was representative of three independent experiments. (E) **Z9j** inhibited the Src kinase in vitro. $n = 3$ (mean \pm SD). *** $p < 0.001$ compared with the control group.

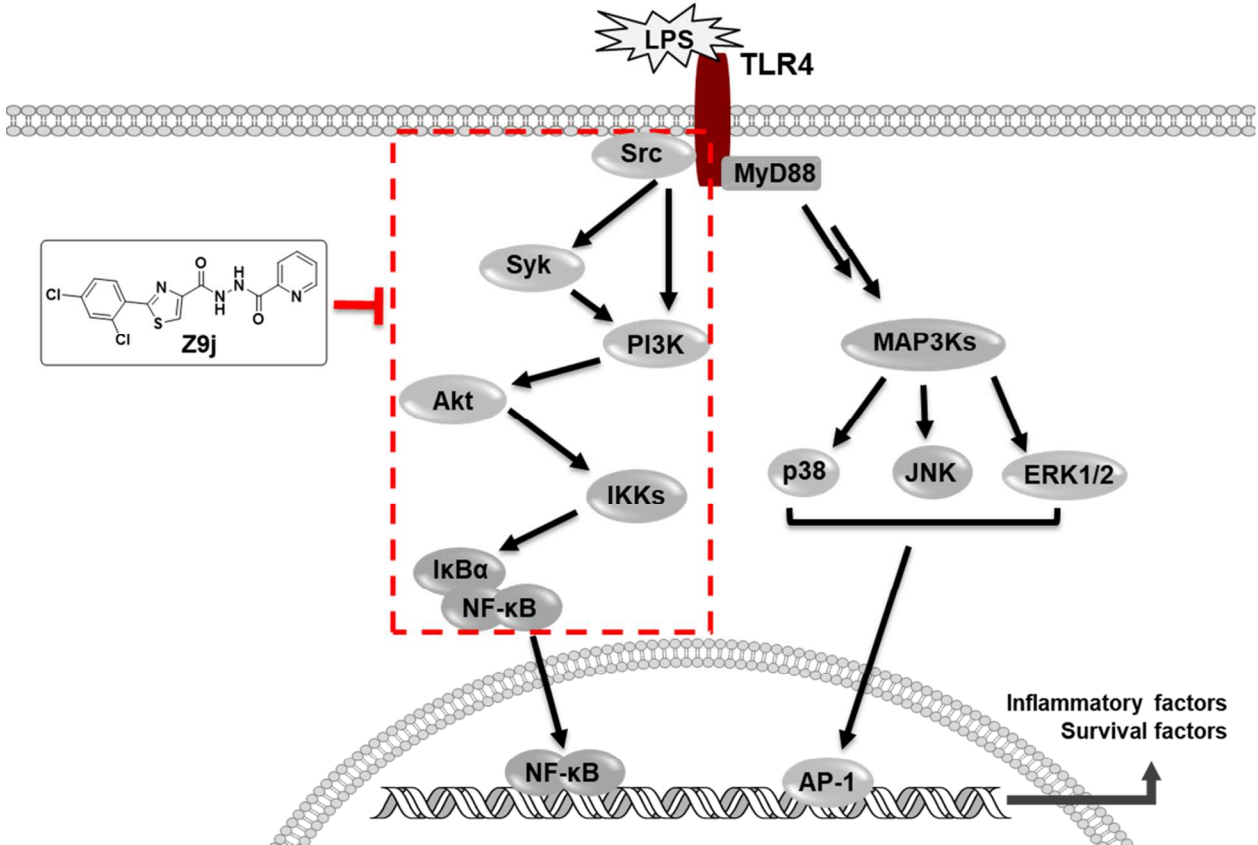


Figure 4. Proposed mechanism by which **Z9j** inhibited NF-κB signaling.

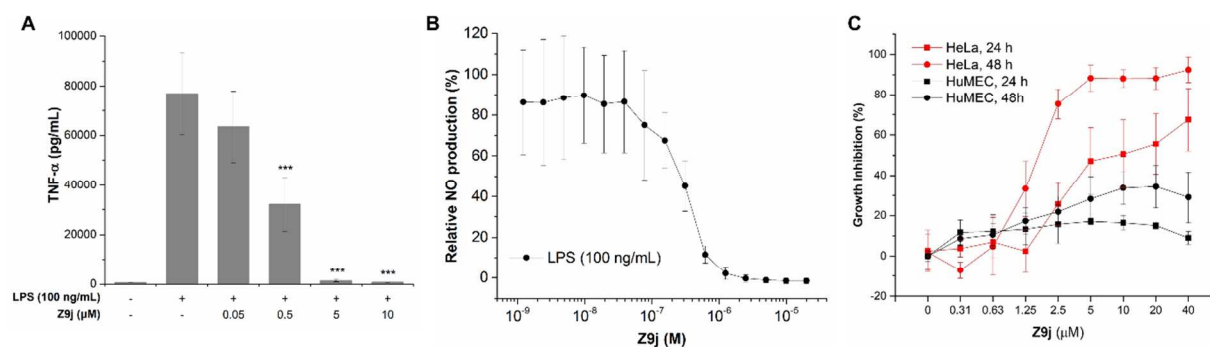


Figure 5. Z9j showed therapeutic potential. (A) Z9j inhibited LPS-induced TNF- α production in RAW 264.7 cells. Cells were pre-treated with increasing amount of Z9j for 30 min and then treated with LPS (100 ng/mL) for 18 h. TNF- α in the media was quantified by ELISA. *** $p < 0.001$ compared with the LPS-only group. (B) Z9j inhibited LPS-induced NO production in RAW 264.7 cells. NO production was evaluated by the DAN assay. $n = 3$ (mean \pm SD). (C) Effects of Z9j on growth of HeLa and HuMEC cells. Exponentially growing cells were treated with the designated concentrations of Z9j for 48 h. Cell viability was tested by measuring the WST-1 absorbance at 450 nm.

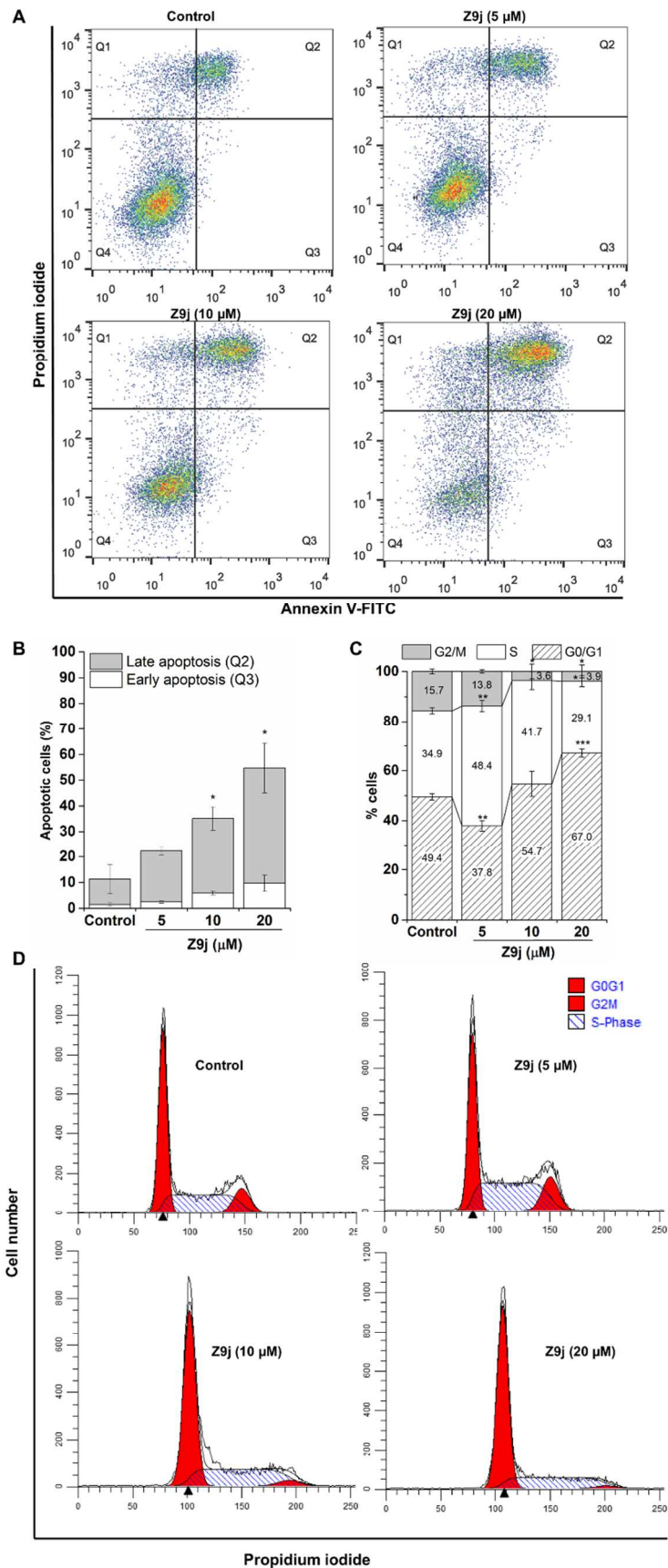


Figure 6. Z9j showed therapeutic potential. (A) Effect of **Z9j** on induction of apoptosis. HeLa cells were treated for 24 h with DMSO control, 5 μ M, 10 μ M, and 20 μ M of **Z9j**. Apoptosis was determined by Annexin V-FITC/PI double staining and flow cytometry. Results shown are representative of three independent experiments. (B) The percentages of early and late apoptotic cells were quantitatively depicted. $*p < 0.05$ compared with the control group. (C) The percentages of cells at each phase are quantitatively depicted. $*p < 0.05$, $**p < 0.01$ and $***p < 0.001$ compared with the control group. $n = 3$ (mean \pm SD). (D) Effect of **Z9j** on cell cycle. HeLa cells were treated for 24 h with DMSO control, 5 μ M, 10 μ M, and 20 μ M of **Z9j**. Cell populations at different phases of the cell cycle were detected using PI staining and flow cytometry analysis. Results shown are representative of three independent experiments.

Table of Contents graphic

